https://doi.org/10.5194/egusphere-2026-1920
Preprint. Discussion started: 18 May 2026

Divergent Land and Ocean Biome Trajectories in a Warming World

Debashis Paul[1], Eun-Jin Park[2], Eun Young Kwon[1,2], Sharif Jahfer[1], Sahil Sharma[1], Mohanan Geethalekshmi Sreeush[3]

[1]Center for Climate Physics, Institute for Basic Science (IBS), Busan, Republic of Korea
[2]School of Carbon Neutrality and Climate Change, Pusan National University, Busan, Republic of Korea
[3]Alfred-Wegener-Institut, Helmholtz-Zentrum für Polar- und Meeresforschung, Bremerhaven, Germany

Correspondence to: Eun Young Kwon (ekwon957@gmail.com)

Abstract. Global biomes, shaped by climate, have long provided a unifying framework for understanding climate change and its impacts on ecosystems and biogeochemical cycles. Using Earth system model projections under continued greenhouse gas emissions, we evaluate global biome redistributions from the present to the year 2300. On land, biomes generally migrate poleward and eastward, whereas in the ocean they exhibit pronounced hemispheric asymmetry, with increasing oligotrophication in the Northern Hemisphere and eutrophication in the Southern Ocean. Terrestrial desert areas are projected to expand moderately, increasing from ~15% to ~20% of the global land surface between 2000 and 2300, with the rate of expansion scaling approximately linearly with global mean warming. In contrast, the simulated extent of oligotrophic ocean regions remains nearly unchanged during the 21st century, after which expansion accelerates, reaching up to 18% of the global ocean by 2300. This nonlinearity arises from phytoplankton's adaptive strategies under nutrient stress—such as atmospheric nitrogen fixation and flexible nutrient uptake ratios—which delay the onset of widespread phosphate limitation. The expansion of terrestrial deserts, and the associated increase in atmospheric iron deposition, further delays the emergence of oligotrophication in some downwind regions. Whereas projections of terrestrial biome changes are broadly consistent across Earth system models, ocean biome projections remain highly divergent, underscoring the critical role of poorly constrained biological processes in shaping marine biogeography and global food security.

1 Introduction

The global distribution of biomes—defined as large-scale ecological regions characterized by distinct climate regimes, dominant life forms, and ecosystem functioning—is a fundamental organizing feature of the Earth system. Anthropogenic climate change and associated environmental pressures are already reshaping terrestrial and ocean biomes, altering the geographic viability of agriculture, fisheries, and biodiversity, with profound implications for food security and regional economies (Walther et al., 2002; Berg et al., 2013; Scheffers et al., 2016). Rapid biome redistribution in recent decades has contributed to local and global species losses, and extinction risks are projected to increase substantially under continued warming (Urban, 2015; Thomas et al., 2004; Penn and Deutsch, 2022). Beyond biodiversity impacts, shifts in biome boundaries modify ecosystem capacities to store carbon, retain water, and recycle nutrients, thereby influencing global hydrological and biogeochemical cycles and feeding back onto climate (Fung et al., 2005). Constraining the trajectory of future biome redistribution is therefore central to understanding long-term Earth system stability and its capacity to sustain human and ecological systems.

Biomes are tightly coupled to climate and have long served as integrative indicators of climatic regimes and their changes (Köppen, 1884; Beck et al., 2023; Geiger, 1954; Fay and Mckinley, 2014; Kaplan et al., 2003; Reid et al., 1978; Palmiéri et al., 2019). On land, vegetation types are strongly controlled by the seasonal evolution of

https://doi.org/10.5194/egusphere-2026-1920
Preprint. Discussion started: 18 May 2026

temperature and water availability, shaped by large scale water–energy balance and atmospheric circulation. This close linkage underpins widely used classification systems such as Köppen's climate zones (Beck et al., 2023; Köppen, 1884; Peel et al., 2007), which relate distinct climate regimes to spatial patterns of terrestrial vegetation. In the ocean, biogeographic provinces are commonly defined using observable variables such as chlorophyll concentration, sea surface temperature, sea-ice cover, and seasonal mixed-layer depth (Fay and Mckinley, 2014; Longhurst, 2007; Palmiéri et al., 2019; Oliver and Irwin, 2008). Because surface chlorophyll and the associated export of organic matter (marine snow) are largely regulated by nutrient supply to the euphotic layer, ocean biomes depend critically on more slowly varying ocean circulation and upper ocean stratification, which are themselves driven by surface winds and air–sea exchanges of heat and freshwater.

At regional scales, ocean biome responses to climate change are shaped by multiple interacting physical and biological feedbacks. In high-nutrient, low-chlorophyll (HNLC) regions and coastal oceans, terrestrial nutrient inputs—via aeolian dust deposition and riverine or groundwater transport—can further influence regional ocean biomes and their variability, highlighting cross-domain coupling between land and ocean systems (Weis et al., 2024; Cho et al., 2018; Mayorga et al., 2010). In oligotrophic regions characterized by severe nutrient depletion, biological feedbacks—such as efficient nutrient recycling, atmospheric N_2 fixation, and flexible cellular nutrient stoichiometry—can buffer biome responses to climate forcing (Kwon et al., 2022; Tanioka and Matsumoto, 2017; Martiny et al., 2022; Galbraith and Martiny, 2015; Bopp et al., 2022; Sreeush et al., 2024). Together, these processes indicate that, although both terrestrial and ocean biomes are climate-sensitive, the dominant mechanisms and timescales governing their responses to climate change differ.

Over the past century, observations reveal widespread poleward and upslope shifts of terrestrial vegetation zones, contraction of cold-adapted ecosystems, and expansion of warm-adapted biomes (Beck et al., 2023; Mahlstein et al., 2013; Kelly and Goulden, 2008; Walther et al., 2002; Loarie et al., 2009; Lohmann et al., 1993). For example, high-latitude and alpine ecotones have exhibited shrub expansion and tree-line advance into tundra regions (Harsch et al., 2009), as well as upward migration of mountain plant communities (Lenoir et al., 2008). Observations and models also indicate broad trends toward expanding drylands and intensifying drought, driven by rising temperatures and altered hydrological cycles (Feng and Fu, 2013; Huang et al., 2016). These changes are generally captured by Earth system model projections, which show consistent poleward migration and desert expansion under 21st-century warming (Beck et al., 2023; Mahlstein et al., 2013; Lohmann et al., 1993). Mechanistic studies attribute subtropical dry-belt expansion and regional aridification to enhanced atmospheric water demand and circulation shifts under anthropogenic warming (Seager et al., 2014; Held and Soden, 2006).

Parallel changes are occurring in the ocean. Marine species are shifting poleward and to greater depths, often at rates exceeding terrestrial shifts due to fewer dispersal barriers (Burrows et al., 2011; Loarie et al., 2009). Basin-scale plankton assemblages have been reorganized in response to ocean warming, including northward displacement of North Atlantic zooplankton communities and tropicalization of temperate reefs (Beaugrand et al., 2002; Vergés et al., 2014). Satellite records further suggest an expansion of oligotrophic subtropical gyres and shifts in phytoplankton biomass under recent warming, although the relatively short observational record limits robust attribution of these

https://doi.org/10.5194/egusphere-2026-1920
Preprint. Discussion started: 18 May 2026

changes (Polovina et al., 2008; Irwin and Oliver, 2009; Leonelli et al., 2022; Boyce et al., 2010). Modeling studies likewise project substantial climate-driven changes in plankton assemblages and biodiversity during the 21st century (Benedetti et al., 2021; Henson et al., 2021; Thomas et al., 2012). While there is broad consensus on warming-driven redistribution, projections of future net primary productivity—an essential source of energy for marine ecosystems—exhibit substantial inter-model spread (Bopp et al., 2013; Kwon et al., 2022; Palmiéri et al., 2019; Laufkötter et al., 2015), with divergence increasing over time (Rodgers et al., 2024). This reflects substantial uncertainties in biological processes and nutrient cycling that strongly influence long-term projections of ocean biome change.

Most existing studies of biome distributions focus on the 21st century, despite the fact that key physical and biological drivers operate on timescales ranging from decades to centuries. Excess heat and carbon stored in the atmosphere and ocean commit the climate system to persistent changes well beyond 2100. Multi-centennial projections indicate continued warming, altered hydrological cycles, strengthened stratification, and long-term circulation changes that may unfold over centuries rather than decades, largely independent of near-term emission pathways (Lee et al., 2025; Randerson et al., 2015; Koven et al., 2022; Sharma et al., 2025; Kug et al., 2022; Peng et al., 2024). Such sustained forcing may therefore trigger nonlinear, threshold-like, or delayed biome reorganizations—particularly in the ocean, where biological adaptation and feedbacks may initially buffer but ultimately amplify structural change. Despite this, a unified and systematic assessment of terrestrial and marine biome evolution beyond the 21st century remains lacking.

Here, we investigate multi-centennial changes in the global distribution of major terrestrial and ocean biomes through the year 2300 using the Community Earth System Model version 2 (CESM2) simulations (Lee et al., 2025), forced by extended Shared Socioeconomic Pathways (SSP) 3-7.0 scenario (Meinshausen et al., 2020). Under this medium–high emission pathway, atmospheric CO_2 rises to ~1515 ppm by 2240—approximately coinciding with the point at which CO_2 emissions decline to zero—and remains elevated thereafter due to the slow uptake of carbon by the ocean and land. This sustained forcing drives continued warming of ~4 °C by 2100 and approximately 10 °C above present-day levels by 2300 (Lee et al., 2025). By jointly analyzing terrestrial and marine biome distributions under prolonged forcing, we extend beyond conventional century-scale assessments to quantify the magnitude, pace, and spatial structure of biome redistribution across the Earth system. This multi-centennial perspective enables us to assess whether land and ocean biomes respond proportionally to warming or diverge structurally over time. Using a 10-member ensemble with different initial conditions, we further examine cross-domain coupling between terrestrial and ocean biomes, with a focus on iron fertilization effects on surface chlorophyll driven by internal variability. Finally, we evaluate the degree of agreement and divergence among Earth system model projections, providing new insights into the robustness and uncertainties of long-term biogeographic responses to sustained greenhouse forcing.

2 Materials and Methods

2.1 Terrestrial biome classifications

We employ the Köppen-Geiger climate classification as modified by Peel et al. (2007) and Beck et al. (2023). For simplicity, we restrict the analysis to the first- and second-level classifications, thereby focusing on broader-scale

https://doi.org/10.5194/egusphere-2026-1920
Preprint. Discussion started: 18 May 2026

climate zones and yielding a total of 15 classes (Table 1). Throughout this study, the terms "climate zones" and "biomes" are used interchangeably. Terrestrial climates are categorized into five primary groups - arid (B), tropical (A), temperate (C), cold (D), and polar (E) - based on mean annual precipitation and surface air temperatures during the hottest and coldest months.

The arid climate zone is identified first, when mean annual precipitation (MAP; mm/year) is lower than a temperature-dependent threshold:

$$\mathrm{MAP} < 10 \times P_{threshold},$$

where,

$$P_{threshold} = \begin{cases} 2 \times \mathrm{MAT}, & \text{if more than 70\% of precipitation falls in winter,} \\ 2 \times \mathrm{MAT} + 28, & \text{if more than 70\% of precipitation falls in summer,} \\ 2 \times \mathrm{MAT} + 14, & \text{otherwise.} \end{cases}$$

Here, MAT denotes mean annual temperature in °C. In the Northern Hemisphere, summer is defined as April-September, whereas in the Southern Hemisphere, it spans October-March. The empirically derived temperature dependence of the aridity threshold implicitly accounts for the strong sensitivity of atmospheric evaporative demand to temperature, which increases rapidly with warming (Held and Soden, 2006). A tropical climate is defined where the temperature of the coldest month (T_{cold}) exceeds 18 °C, whereas a polar climate is defined where the temperature of the hottest month (T_{hot}) remains below 10 °C. Regions lying between these two regimes are classified as temperate when $T_{cold} > 0$ °C, and as cold when $T_{cold} < 0$ °C. The temperate and cold climates broadly correspond to maritime and continental climates, respectively, reflecting the contrasting influence of oceanic and terrestrial heat capacity on winter air temperatures in downstream regions.

Each main climate group is further subdivided based on precipitation seasonality and magnitude. Arid climates are subdivided into desert ($\mathrm{MAP} < 5 \times P_{threshold}$) and steppe ($\mathrm{MAP} \geq 5 \times P_{threshold}$). Tropical climates are subdivided into rainforest, monsoon, and savannah, based on precipitation in the driest month (P_{dry}; mm/month): rainforest ($P_{dry} \geq 60$ mm/month), monsoon ($P_{dry} \geq 100 - \mathrm{MAP}/25$), and savannah ($P_{dry} < 100 - \mathrm{MAP}/25$), where the classification into rainforest precedes over the ones into monsoon or savannah. Temperate and cold climates are subdivided into dry summer, dry winter, or wet (no dry season) regimes, depending on seasonal precipitation contrasts. A region is classified as dry summer when precipitation in the driest summer month (P_{sdry}; mm/month) satisfies the criteria of both $P_{sdry} < 40$ mm/month and $P_{sdry} < P_{wwet}/3$, where P_{wwet} is precipitation in the wettest winter month in mm/month. A region is classified as dry winter when precipitation in the driest winter month (P_{wdry}) satisfies the criterion of $P_{wdry} < P_{swet}/10$, where P_{swet} is precipitation in the wettest summer month in mm/month. Regions that meet neither criterion are classified as having no dry season (i.e., wet).

Finally, polar climates are subdivided into tundra, where the warmest month temperature exceeds 0 °C, and frost, where the warmest month temperature remains below 0 °C. The classification criteria are summarized in Table 1.

https://doi.org/10.5194/egusphere-2026-1920
Preprint. Discussion started: 18 May 2026

143 Table 1 Classification of Terrestrial Biomes

Land biomes (main groups)	Criteria for main groups[a]	Land biomes (subgroups)	Criteria for subgroups[a]
Tropical (A)	Not (B) & $T_{cold} \geq 18$	Rainforest (f)	$P_{dry} \geq 60$
		Monsoon (m)	Not (Af) & $P_{dry} \geq 100 - MAP/25$
		Savannah (w)	Not (Af) & $P_{dry} < 100 - MAP/25$
Arid (B)	$MAP < 10 \times P_{threshold}$	Desert (W)	$MAP < 5 \times P_{threshold}$
		Steppe (S)	$MAP \geq 5 \times P_{threshold}$
Temperate (C)	Not (B) & T_{hot}>10 & 0< T_{cold} < 18	Dry summer (s)	$P_{sdry} < 40$ & $P_{sdry} < P_{wwet}/3$
		Dry winter (w)	$P_{wdry} < P_{swet}/10$
		Wet (f)	Not Cs or Cw
Cold (D)	Not (B) & T_{hot}>10 & $T_{cold} \leq 0$	Dry summer (s)	$P_{sdry} < 40$ & $P_{sdry} < P_{wwet}/3$
		Dry winter (w)	$P_{wdry} < P_{swet}/10$
		Wet (f)	Not Ds or Dw
Polar (E)	Not (B) & $T_{hot} \leq 10$	Tundra (T)	$T_{hot} > 0$
		Frost (F)	$T_{hot} \leq 0$

144 [a]For units and descriptions, we refer readers to the text or Beck et al. (2023).

145 **2.2 Ocean biome classifications**

146 Ocean biomes are defined using the annual maximum surface chlorophyll concentration and the annual maximum
147 mixed-layer depth, following the framework of Palmiéri et al. (2019). As a modification to that framework, we
148 additionally include a sea-ice biome, defined by the annual minimum sea-ice fraction exceeding 0.5 (Fay and Mckinley,
149 2014). This approach categorizes the global ocean surface into seven biomes, with a primary focus on the distribution
150 of open-ocean phytoplankton functional groups that form the foundation of marine ecosystems. After identifying the
151 sea-ice biome, the remaining ocean surface is grouped into oligotrophic, submesotrophic, mesotrophic, and eutrophic
152 biomes, ordered by increasing annual maximum surface chlorophyll concentration (Chl; mg/m^3) (Table 2). The
153 oligotrophic biome is defined where Chl < 0.075 mg/m^3, similar to a threshold used by Polovina et al. (2008). These
154 regions represent the least productive areas of the open ocean and are broadly analogous to arid deserts on land. The
155 submesotrophic biome, defined where 0.075 mg/m^3 ≤ Chl < 0.25 mg/m^3, represents moderately low-productivity

https://doi.org/10.5194/egusphere-2026-1920
Preprint. Discussion started: 18 May 2026

ocean regions and the upper bound of 0.25 mg/m^3 has previously been used to distinguish subtropical from subpolar ocean regimes (Fay and Mckinley, 2014).

The mesotrophic and eutrophic biomes are further subdivided according to winter mixed-layer depth, distinguishing regions with deep (≥ 100 m) from shallow (< 100 m) winter mixing. This separation differentiates perennially stratified low-latitude systems from mid- and high-latitude regions where winter convection deepens the mixed layer and enhances seasonal nutrient supply. This subdivision enables us to refine productive ocean regions based on the strength of seasonal control over nutrient entrainment and primary productivity.

The spatial extent and global distribution of individual biomes are sensitive to the choice of chlorophyll thresholds, the seasonal metric used to define productivity (Polovina et al., 2008; Irwin and Oliver, 2009; Leonelli et al., 2022), and whether surface or euphotic-depth-averaged chlorophyll is employed. Nevertheless, the qualitative features of long-term biome redistributions from the present to the year 2300 remain robust to these methodological choices, as discussed in next sections.

Table 2 Classification of Ocean Biomes

Ocean biomes[a]	Annual minimum sea-ice (ICE)	Annual maximum chlorophyll (Chl) Unit in mg/m^3	Annual maximum mixed layer depth (MLD) Unit in m
Sea-ICE	ICE < 0.5	----	----
Oligotrophic	----	Chl < 0.075	----
Submesotrophic	----	0.075 ≤ Chl < 0.25	----
Mesotrophic	----	0.25 ≤ Chl < 1.0	MLD ≥ 100
Low-mixing mesotrophic	----	0.25 ≤ Chl < 1.0	MLD < 100
Eutrophic	----	Chl ≥ 1.0	MLD ≥ 100
Low-mixing eutrophic	----	Chl ≥ 1.0	MLD < 100

[a]For biome names and threshold values, we largely follow Palmiéri et al. (2019).

2.3 Observational datasets

To verify the present-day distributions of terrestrial and ocean biome distributions simulated by our model, we compare our estimates with those from observational and reanalysis data products. Monthly temperature and precipitation are obtained from the fifth-generation European Centre for Medium-Range Weather Forecasts (ECMWF) reanalysis, ERA-5, for the period of 1981-2010 (Hersbach et al., 2020). For ocean biomes, we use monthly mean surface chlorophyll concentrations derived from the Sea-viewing Wide Field-of-view Sensor (SeaWiFS) satellite for the period of 2000-2010 (O'reilly et al., 1998). Annual maximum chlorophyll concentrations are computed for each year and then averaged over the 11-year period. We also use a monthly mean mixed-layer depth climatology estimated from Argo float profiles and in-situ observations (De Boyer Montégut, 2023; De Boyer Montégut et al., 2004) to determine the monthly maximum mixed-layer depth. The sea-ice concentration to identify the sea-ice biome is

https://doi.org/10.5194/egusphere-2026-1920
Preprint. Discussion started: 18 May 2026

obtained from National Snow and Ice Data Center (NSIDC) Climate Data Record (Meier et al., 2021), as incorporated into the E.U. Copernicus Marine Service Information (CMEMS) Global Ocean Ensemble Physics Reanalysis for the period of 2000-2010. Annual minimum sea-ice concentrations are computed for each year and then averaged over the 11-year period.

2.4 CESM2 multi-centennial simulations

The primary model analyzed in this study is the CESM2, a fully coupled global Earth system model that explicitly simulates interactions among the atmosphere, ocean, sea-ice, and land components (Danabasoglu et al., 2020). The atmospheric component is the Community Atmosphere Model version 6 (CAM6), which includes updated parameterizations of cloud microphysics, aerosol-cloud interactions, and radiative transfer, and is coupled to the Community Land Model version 5 (CLM5). CLM5 explicitly represents land-use change, snow and hydrological processes, and terrestrial geophysical and biogeochemical cycles (Lawrence et al., 2019). Sea-ice processes are simulated using the Community Ice CodE (CICE) version 5.1.2 (CICE5), which includes multi-category ice thickness distributions, melt pond physics, and improved thermodynamic and dynamic formulations (Hunke et al., 2015).

The ocean component is the Parallel Ocean Program version 2 (POP2) (Smith et al., 2010), which simulates ocean circulation, mixing, and tracer transport. Ocean biogeochemistry is represented by the Marine Biogeochemistry Library (MARBL), which resolves coupled carbon, nitrogen, phosphorus, iron, and silica cycles, air–sea CO_2 exchange, and lower-trophic marine ecosystem dynamics (Long et al., 2021). MARBL includes three explicit phytoplankton functional types (diatoms, small phytoplankton, and N_2-fixing diazotrophs), one implicit calcifying phytoplankton, a single zooplankton functional group, along with parameterizations of organic matter production, export, and remineralization. Importantly, MARBL incorporates adaptive phytoplankton physiological traits, such as variable C:P stoichiometry and flexible nutrient utilization pathways, enabling dynamic ecosystem responses to changing environmental conditions (Long et al., 2021; Galbraith and Martiny, 2015; Moore et al., 2004). The nominal horizontal resolution of all CESM2 components is approximately 1° × 1°, with enhanced vertical resolution (10 m) in the upper ocean (top 160 m).

CESM2 simulations were conducted from 1850 to 2014 under historical radiative and land-use forcing, and from 2015 to 2100 following the SSP3-7.0 scenario (O'neill et al., 2016), employing a 100-member large ensemble (CESM2-LE) (Rodgers et al., 2021). To explore long-term, multi-centennial responses, the simulations were extended from 2101 to 2500 using 10 ensemble members (Lee et al., 2025), following the extended SSP3-7.0 forcing protocol (Meinshausen et al., 2020). While greenhouse gas concentrations follow the prescribed trajectories in Meinshausen et al. (2020), land-use change and aerosol forcing are held fixed at their 2100 levels throughout the extended simulations. We refer readers to Lee et al. (2025) for details of the simulations and an overview of the projected climate and biogeochemical changes. Because the climate system approaches a quasi-equilibrium state under stabilized forcing during 2300–2500, our analysis focuses on the period 1980-2300. We define 30-year climatological means centered on 1980-2010, 2071-2100, and 2271-2300 to represent the present, near future, and extended future, respectively. Unless otherwise noted, climatological biome distributions are derived from a single ensemble member.

https://doi.org/10.5194/egusphere-2026-1920
Preprint. Discussion started: 18 May 2026

It is important to note that the terrestrial biome distributions diagnosed here are not identical to the vegetation types explicitly represented in CLM5 (Lawrence et al., 2019). In CLM5, each land grid cell is partitioned into six land units—vegetated, crop, urban, lake, glacier, and wetland—with fractional coverage prescribed and evolving over time according to historical and future land-use datasets (Lawrence et al., 2016; Danabasoglu et al., 2020). Within the vegetated land unit, vegetation is represented by multiple plant functional types (PFTs) that differ in photosynthetic pathway, phenology, physiology, and bioclimatic niche, including needleleaf and broadleaf trees, shrubs, and C_3 and C_4 grasses (Lawrence et al., 2019). Transitions among the PFTs, as well as their physiological state and function — including net primary production, leaf area index, and nitrogen and carbon pools —are simulated prognostically in response to climate conditions and atmospheric CO_2 levels.

By contrast, the Köppen–Geiger climate classification applied here is derived solely from simulated near-surface temperature and precipitation, and is therefore not necessarily consistent with prescribed land-use fractions or simulated vegetation structure and function. Accordingly, the climate-based biomes diagnosed in this study should be interpreted as indicators of climatic suitability rather than direct representations of vegetation distribution simulated by CLM5.

We further note that the CESM2 configuration employed in this study does not include a dynamic land-ice module (Lipscomb et al., 2019). Instead, surface air temperature and land-ice accumulation and ablation are calculated using the surface mass and energy balance scheme implemented in CLM5, which represents subgrid-scale topographic variability through multiple elevation classes over glaciated grid cells (Lipscomb et al., 2013; Danabasoglu et al., 2020). As a result, dynamic ice-sheet processes such as ice flow and ice-climate feedback are not represented. Therefore, diagnosed terrestrial polar frost biomes over Greenland and Antarctica should be interpreted in light of this modeling limitation.

2.5 Other Earth system models

To assess the sensitivity of projected biome redistributions to Earth system model formulation, we additionally analyze multi-centennial simulations from two other Earth system models participating in the Coupled Model Intercomparison Project Phase 6 (CMIP6) (Eyring et al., 2016): the Canadian Centre for Climate Modelling and Analysis fifth-generation Earth System Model (CanESM5) (Swart et al., 2019) and the UK Earth System Model version 1 (UKESM1) (Sellar et al., 2019). These models span a range of structural complexity and process representations, particularly in their treatments of atmospheric chemistry, aerosol-cloud interactions, and coupling of terrestrial and marine biogeochemical cycles (Christian et al., 2022; Yool et al., 2013). Notably, differences in the formulation and parameterization of marine biogeochemical modules lead to substantial variation in simulated nutrient cycling, primary production, and ecosystem structure, as documented in previous intercomparison studies (Bopp et al., 2013; Kwiatkowski et al., 2020; Laufkötter et al., 2015).

We also analyze simulations from the CESM2 Whole-Atmosphere Configuration version 6 (CESM2-WACCM6) (Koven et al., 2022; Danabasoglu et al., 2020). CESM2-WACCM6 differs from the standard CESM2 configuration by employing WACCM6 in place of CAM6, thereby extending the atmospheric domain into the

https://doi.org/10.5194/egusphere-2026-1920
Preprint. Discussion started: 18 May 2026

mesosphere and lower thermosphere and explicitly representing interactive stratospheric chemistry and dynamics (Koven et al., 2022; Danabasoglu et al., 2020).

Across the three Earth system models, climate sensitivity and carbon-cycle responses to CO_2 forcing vary substantially (Meehl et al., 2020; Koven et al., 2022), providing a useful range of structural and feedback uncertainties for intercomparison. Because extended future simulations under SSP3-7.0 are not available for these additional models, we instead analyze simulations conducted under the SSP5-8.5 scenario. SSP5-8.5 represents a high-emissions pathway in which radiative forcing reaches approximately 8.5 W m^{-2} above preindustrial levels by 2100, compared with 7.0 W m^{-2} under SSP3-7.0 (O'neill et al., 2016). For each model, only a single ensemble realization is available over the analysis period. To facilitate intercomparison, all model outputs are regridded to a common 1° × 1° horizontal grid prior to biome diagnostics.

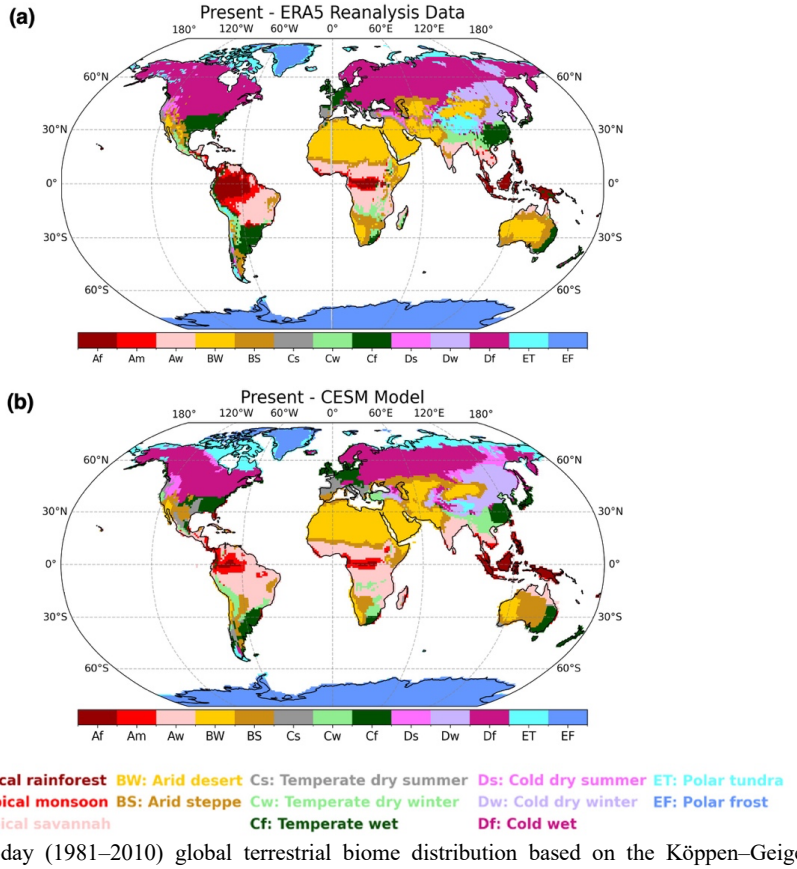

Figure 1: Present-day (1981–2010) global terrestrial biome distribution based on the Köppen–Geiger climate classification, comparing (a) ERA5 reanalysis with (b) Community Earth System Model version 2 (CESM2) simulations.

3 Projected changes in terrestrial biome distribution

3.1 Observed and simulated terrestrial biome distributions

https://doi.org/10.5194/egusphere-2026-1920
Preprint. Discussion started: 18 May 2026

CESM2 broadly reproduces the present-day terrestrial biome distribution, as estimated from a reanalysis-based climatology averaged over 1981-2010 (Fig. 1). Tropical rainforests are concentrated along the Intertropical Convergence Zone, where persistently warm and wet conditions sustain dense forests in the Amazon, Congo Basin, and Maritime Continent. These rainforest regions typically transition into relatively narrow tropical monsoon zones, which are in turn bordered by broader tropical savannahs across South America and Africa. Outside the tropics, arid deserts and steppes dominate the subtropic belts near 30° N and 30° S, where the descending branches of the Hadley and Ferrel circulations drive moisture divergence. These dry climates are prominent across the Sahara, the Middle East, and much of Australia (except along the northern and eastern coasts).

Polar tundra is found in high northern latitudes or in high-elevation mountain regions, while polar frost covers Antarctica and interior of Greenland. At mid to high latitudes outside the polar regions, large areas of North America and Eurasia are primarily characterized by wet climates with severe winters (i.e., cold-wet or continental-wet climates). In contrast, wet climates with relatively mild winters (i.e., temperate-wet or maritime-wet climates) occur mainly along the eastern margins of continents around 30°S and 30°N, where the influence of warm western boundary currents enhances heat and moisture transport. A notable exception is the northwestern Europe around 45°N, where the combined influence of North Atlantic Current and frequent mid-latitude storm activity maintains year-round wet conditions with mild winters.

Notable differences between simulated and observed biome distribution include an underestimation of tropical rainforest extent and a corresponding overestimation of tropical savannahs (Fig. 1), primarily attributable to biases in simulated precipitation during the driest month (Fig. S1). In addition, cold biases in simulated hottest-month temperatures lead to an overly extensive polar tundra that encroaches upon cold-wet climate zones in the northernmost regions of North America and Eurasia. Conversely, polar tundra is underestimated in high-mountain regions such as the Andes and Himalaya, reflecting the model's coarse horizontal resolution and limited ability to resolve steep topographic gradients. Seasonal precipitation biases further contribute to an overestimation of dry-summer climate regimes in both temperate and cold climate zones, at the expense of temperate- and cold-wet climates. Although these regional biases produce discrepancies in aggregated biome areas, reaching up to ~5% of the global land surface (Fig. 2a), the model reproduces the first-order spatial patterns of observed terrestrial biomes reasonably well, providing confidence in its projected future changes.

3.2 Near-future changes in terrestrial biome distribution

Consistent with previous studies (Beck et al., 2023; Mahlstein et al., 2013; Lohmann et al., 1993), our 21st century projections indicate a contraction of polar tundra and frost zones, accompanied by poleward expansions of arid and tropical climate zones. These shifts are evident in projected changes in aggregated biome areas (Figs. 2a and 2b) and in the spatial patterns of terrestrial climate zones (Fig. 3a). Figures 2 and 3 additionally present hypothetical estimates in which only temperature or precipitation is allowed to vary, while the other variable is held fixed at present-day conditions. These estimates enable attribution of the projected biome changes to individual climate drivers, as discussed below.

https://doi.org/10.5194/egusphere-2026-1920
Preprint. Discussion started: 18 May 2026

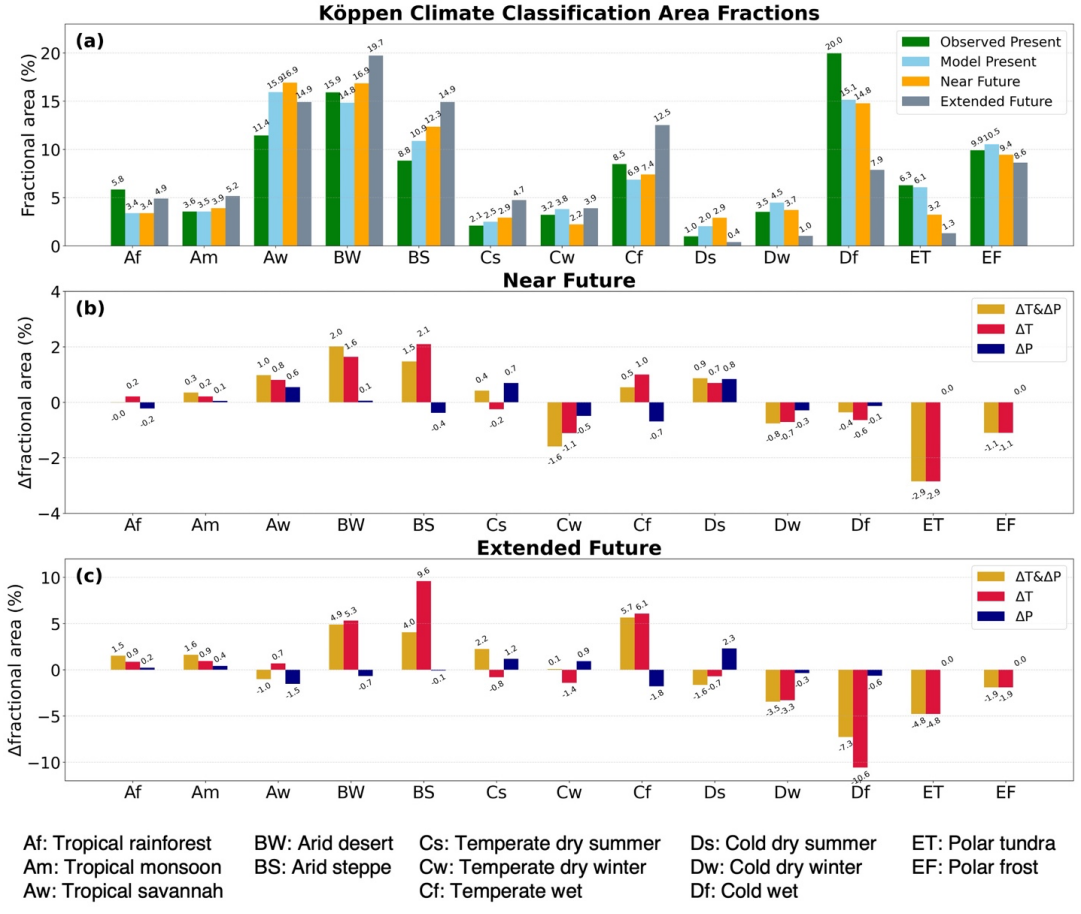

Figure 2: Globally integrated terrestrial biome areas and their projected future changes. (a) Fractional land area occupied by each terrestrial biome under four cases: observed present-day conditions (ERA5), simulated present-day conditions, near-future projections, and extended-future projections. (b–c) Attribution of projected changes in biome fractional areas to individual climate drivers for the (b) near-future and (c) extended-future periods, relative to the present day. Simulated full changes are shown in yellow bars (ΔT&ΔP), while two hypothetical sensitivity estimates are shown for temperature changes alone (ΔT; red) and precipitation changes alone (ΔP; blue). The hypothetical estimates are derived by allowing only temperature (precipitation) to vary, while precipitation (temperature) is held fixed at present-day values. Numerical values corresponding to the y-axis are provided above each bar.

Among the major shifts, arid deserts and steppes exhibit the largest net expansion, increasing by 3.5 % points relative to a present-day coverage of 24% (Fig. 2a). This expansion is driven by both warming-induced increases in the aridity threshold and, in some regions, reductions in mean annual precipitation (Figs. 3a-3c and S2). In contrast, polar tundra and frost zones experience the most pronounced net decline, decreasing by 4.0 % points from a present-day value of 17%, consistent with accelerated high-latitude warming and enhanced permafrost thaw (Kim et al., 2024).

https://doi.org/10.5194/egusphere-2026-1920
Preprint. Discussion started: 18 May 2026

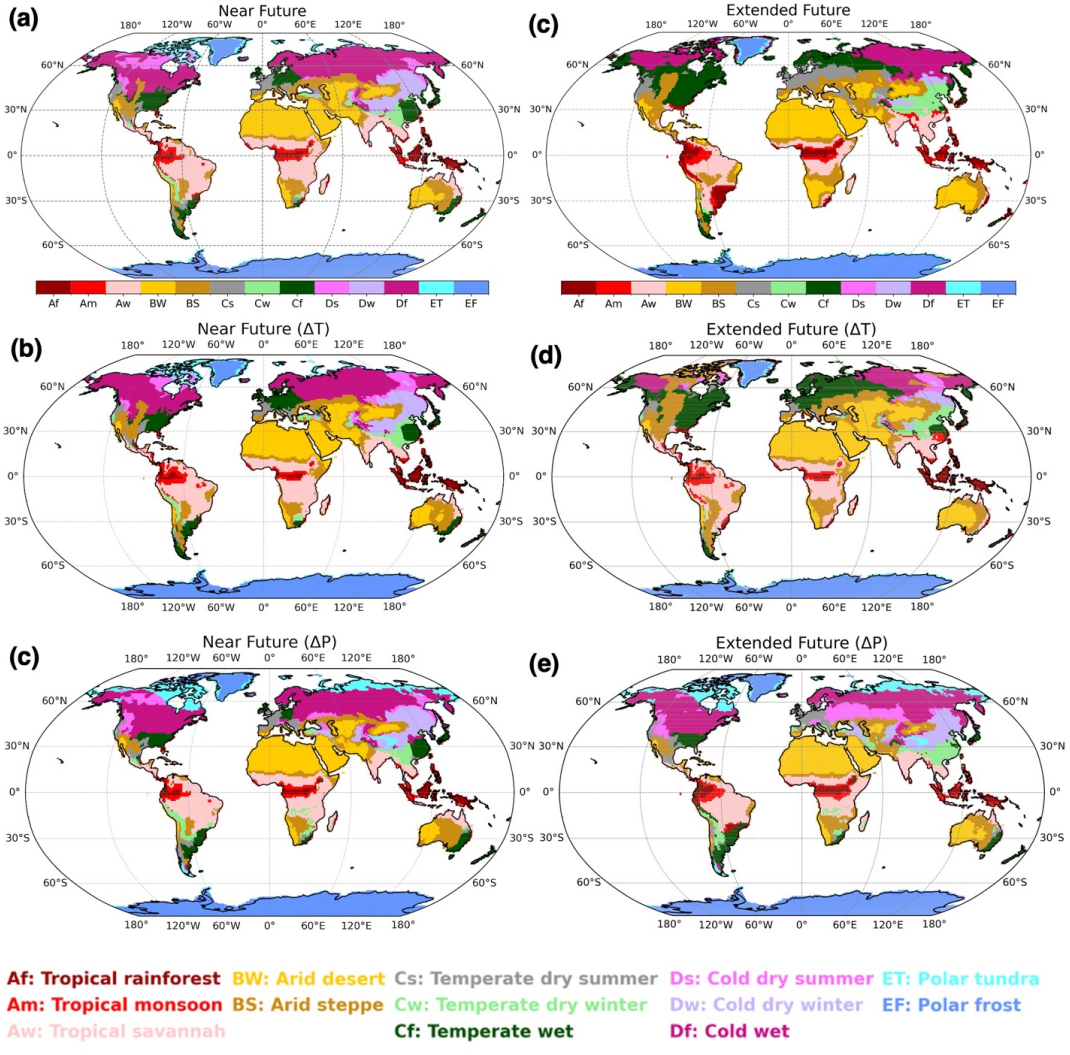

Figure 3: Spatial distribution of terrestrial biomes in the near and extended futures based on the Köppen-Geiger classification. (a) Simulated biome distribution for the near-future period (2071-2100). (b) Hypothetically estimated biome distribution for the near future assuming that only temperature changes, while precipitation is held fixed at present-day values. (c) Hypothetically estimated biome distribution for the near future, assuming that only precipitation changes, while temperature is held fixed at present-day values. (d-f) Same as (a-c), but for the extended-future period (2271-2300).

Tropical climate zones exhibit a comparatively modest expansion by 2100, with a net increase of 1.3% points from the present-day value of 23% (Fig. 2a). This increase is predominantly driven by the expansion of tropical savannah climates, which account for approximately 1.0 % point of this increase. Temperate and cold climate zones generally shift poleward, consistent with global warming patterns (Figs. 3a-3c and S3). Because northward expansion

https://doi.org/10.5194/egusphere-2026-1920
Preprint. Discussion started: 18 May 2026

of northern boundaries is largely offset by contraction at their southern boundaries, net areal changes in temperate and cold zones remain small. While surface warming is the dominant driver of these shifts, changes in precipitation play an important role in redistributing climate subgroups. For example, enhanced summer drying over northern Canada and eastern Europe (Fig. S4) contribute to regional expansion of temperate and cold dry-summer climate zones (Fig. 3c).

3.3 Extended future changes in terrestrial biome distribution

The reorganization of terrestrial biomes intensifies beyond the 21st century (Figs. 2 and 3d-3f), when cumulative atmospheric carbon and global surface temperatures reach their maxima and remain elevated (Lee et al., 2025). Persistent surface warming raises the aridity threshold (Fig. S2), driving continued expansion of arid climate zones from 29% of the global land surface during the near-future period to 35% in the extended-future period. Arid deserts alone expand from 15% of global land area under present-day conditions to 17% in the near future and 20% in the extended future, emerging as the dominant terrestrial biome in our projections.

Regionally, accelerated surface warming combined with enhanced dryness drives an eastward expansion of arid climates across Southern Africa and Australia, occupying large portions of these continents (Figs. 3d-3f and S2). In the Northern Hemisphere, a projected collapse of the Atlantic Meridional Overturning Circulation (AMOC) (Lee et al., 2025), together with poleward shifts of subtropical high-pressure systems (Fig. S5), promote perennial drying and facilitates a transition toward arid conditions across the Mediterranean region (Fig. 3d). By contrast, over mid-continental North America and Eurasia, where mean annual precipitation increases, the expansion of arid climates is primarily governed by warming-induced increases in the aridity threshold rather than by precipitation reductions (Fig. S2).

Polar biomes continue to contract from the near future to the extended future, with permafrost-free conditions emerging by ~2150 (Lee et al., 2025) (Figs. 2c and 3d-3f). At the opposite end of the climate spectrum, tropical rainforest and monsoon climates expand in response to projected increases in precipitation during the climatologically driest month, together with accelerated surface warming (Fig. S3). This expansion occurs at the expense of tropical savannah and temperate wet climates. Notably, tropical rainforest climates extend beyond the conventional tropical belt bounded by 30°N and 30°S, emerging in extratropical coastal regions including the east coasts of the United States, South Korea, and Australia, as well as coastal regions of Japan and New Zealand.

Another prominent feature of the extended future is the accelerated conversion of cold climate regimes to temperate ones, particularly across northwestern Eurasia and eastern North America (Figs. 3d-3f), where coldest-month temperatures exceed the 0 °C threshold. Across western to central Eurasia near 50°N, projected hydroclimatic changes are characterized by drier summers and wetter winters (Fig. S4), shifting climates toward temperate dry-summer regimes. Taken together, temperate climates currently confined to western Europe extend eastward into central Russia, leading to a substantial reduction in cold wet climate zones, whose areal extent declines from approximately 15% of global land area in the near future to 8% in the extended future (Fig. 2a).

https://doi.org/10.5194/egusphere-2026-1920
Preprint. Discussion started: 18 May 2026

4 Projected changes in ocean-biome distributions

4.1 Present-day distributions and the sensitivity to classification metrics

Observation-based estimates indicate that eutrophic biomes with strong seasonal mixing occur in the subpolar gyres of the North Atlantic and the Northwest Pacific, as well as in localized regions of the Antarctic Circumpolar Current (ACC) (Fig. 4a), where deep winter convection entrains subsurface nutrients into the euphotic zone. By contrast, eutrophic biomes without pronounced seasonal mixing are found primarily in eastern boundary upwelling systems, the Somali upwelling region, and other coastal zones influenced by wind-driven upwelling and enhanced nutrient inputs from terrestrial runoff and shelf sediments. Beyond these high-productivity coastal regions, subpolar gyres are dominated by mesotrophic biomes, while subtropical gyres are mainly occupied by submesotrophic biomes. At the centers of the subtropical gyres, oligotrophic biomes dominate, reflecting perennially nutrient-depleted surface waters maintained by wind-driven Ekman convergence and strong upper-ocean stratification.

CESM2 reproduces these observed large-scale patterns of ocean biome distribution, simulating oligotrophic and submesotrophic biomes across broad regions of subtropical gyres, and mesotrophic and eutrophic biomes along the equator, in coastal upwelling zones, and across subpolar gyres and the Southern Ocean (Fig. 4b). These biome classifications broadly reflect the simulated biogeography of phytoplankton functional types and their associated nutrient cycles (Fig. S6). Eutrophic biomes are dominated by fast-growing, large phytoplankton that benefit from rapid nutrient supply through vertical mixing and upwelling, whereas submesotrophic to mesotrophic biomes are typically associated with small phytoplankton exhibiting high nutrient affinity under low-nutrient conditions. Diazotrophs capable of biological N_2 fixation are largely restricted to warm, low-latitude regions, reflecting strong temperature constraints, with optimal growth occurring above approximately 15 °C (Long et al., 2021). As expected, oligotrophic biomes exhibit the lowest phytoplankton biomass.

Despite the broad agreement between the observation-based estimate and the model simulations, several notable discrepancies remain (Fig. 4b), reflecting limitations in simulating the ocean's physical and biogeochemical states (Long et al., 2021; Danabasoglu et al., 2020). The most prominent bias is a systematic overestimation of annual maximum chlorophyll concentrations over much of the global ocean, particularly in upwelling-dominated regions (Fig. S7). This bias inflates the simulated areal extent of eutrophic biomes in the mid- to high- latitudes, where observations instead suggest predominantly mesotrophic conditions. In addition, slight chlorophyll overestimation across large portions of subtropical gyres leads to a substantial underestimation of oligotrophic biome extent. Specifically, the simulated oligotrophic biome occupies only 0.4% of the global ocean under present-day conditions, whereas observations suggest a coverage of approximately 8%. The model also underestimates the annual maximum mixed-layer depth across the mid- to high-latitudes of both hemispheres (Fig. S7), resulting in an underestimation of seasonally high-mixing mesotrophic biomes (Fig. 4b). Furthermore, warm biases in polar oceans lead to smaller simulated sea-ice biome extents compared with observations.

https://doi.org/10.5194/egusphere-2026-1920
Preprint. Discussion started: 18 May 2026

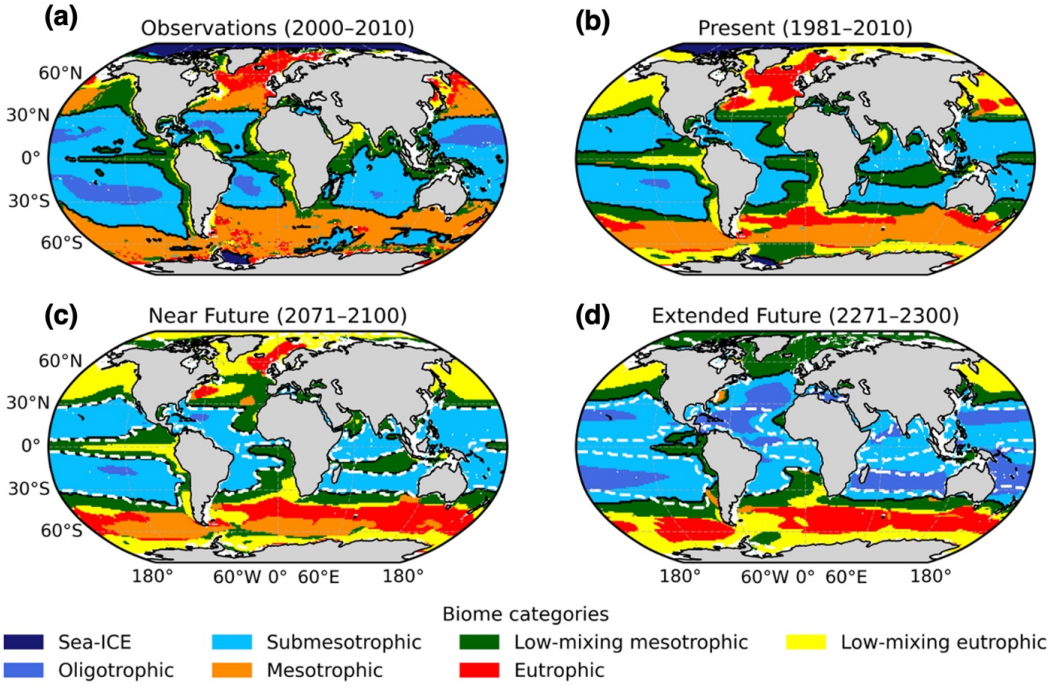

Figure 4: Present-day distributions of ocean biomes and their projected future changes based on the classification summarized in Table 2. (a) Observed ocean biome distribution for 2000-2010. (b) Simulated present-day distribution for 1981-2010. (c) Near-future projection for 2071-2100. (d) Extended-future projection for 2271-2300. For the simulated cases (b-d), ocean biomes are classified using surface chlorophyll concentrations averaged over the upper 10 m of the ocean model. The white dashed lines in (c) and (d) denote the simulated present-day boundary between submesotrophic and mesotrophic biomes, defined by a chlorophyll threshold of 0.25 mg/m^3 and taken from (b).

It is further to note that ocean biome classification is highly sensitive to whether chlorophyll concentration is defined at the surface (the upper 10 m in the ocean model) or averaged over the euphotic zone, defined as the layer within which photosynthetically available radiation remains more than 1% of its surface value. When euphotic-depth-averaged chlorophyll is used, the estimated areal extents of oligotrophic and submesotrophic biomes increase substantially relative to the surface-based metric, from 0.4% to 14% and from 40% to 54% of the global ocean, respectively (Fig. S8). Although the oligotrophic area becomes more comparable to observations under this definition, the euphotic-depth-averaged metric produces unrealistically extensive submesotrophic biomes in the Southern Ocean, a feature not supported by observations. This strong sensitivity arises from pronounced vertical variability in chlorophyll concentration in the stratified ocean, associated with vertical variability in phytoplankton biomass, photoacclimation, and grazing pressure (Cullen, 2015; Cornec et al., 2021), processes represented in the model to some extent (Long et al., 2021). In contrast, subpolar regions of the Northern Hemisphere, which are characterized by strong seasonal vertical mixing, show relatively weak sensitivity to the choice of chlorophyll metric. Because chlorophyll concentrations in the lower euphotic zone do not necessarily correspond to phytoplankton biomass, we

https://doi.org/10.5194/egusphere-2026-1920
Preprint. Discussion started: 18 May 2026

therefore adopt the surface chlorophyll-based metric as our primary diagnostic. Nevertheless, we assess and discuss the sensitivity of our key results to the use of euphotic-depth-averaged chlorophyll.

4.2 Future changes in ocean biome distribution

Projected reorganizations of global ocean biomes exhibit a pronounced hemispheric asymmetry (Figs. 4c-4d), driven by ocean circulation responses to greenhouse warming. In the North Atlantic subpolar gyre, surface warming and freshening enhance upper-ocean stratification and weaken the AMOC, reducing the supply of nutrients to the surface. As a result, oligotrophic and submesotrophic biomes expand northward into the region currently characterized by the North Atlantic subpolar front. In contrast, much of the Southern Ocean becomes increasingly eutrophic, as poleward-intensified westerlies enhance nutrient supply through increased vertical mixing and lateral advection (Misumi et al., 2014). The poleward migration of deep winter convection bands (Fig. S9), associated with shifts in the westerlies (Fig. S5), further drive the poleward expansion of diatom-dominated eutrophic biomes (Fig. S6).

Despite these contrasting responses at northern and southern high latitudes, both Arctic and Antarctic sea-ice biomes transition to eutrophic states by the end of the 21st century (Fig. 4c), coincident with the projected loss of summer sea ice (Fig. S9). From the near to extended future, both polar regions remain productive, while the Arctic shifts predominantly toward mesotrophic conditions by 2300 (Fig. 4d). Another hemispherically symmetric feature is the widespread emergence of oligotrophic biomes, which replace present-day submesotrophic biomes in the subtropical gyres from the near to extended future. Using the surface chlorophyll-based metric, oligotrophic biomes expand from 0.4% of the global ocean at present to 0.8% in the near future and further to 18% in the extended future. This pronounced post-2100 oligotrophication is robust to the choice of chlorophyll metric: when the oligotrophy threshold is applied to euphotic-depth-averaged chlorophyll, oligotrophic biome coverage increases from 14% at present to 19% in the near future and to 44% in the extended future (Fig. S8). In the extended future, these expanded oligotrophic biomes are largely devoid of all major phytoplankton functional groups (Fig. S6). The most pronounced decline occurs in diazotrophs, underscoring their critical role in supplying bioavailable nitrogen to the euphotic zone and, consequently, in sustaining marine ecosystems (Bopp et al., 2022).

5 Divergent trajectories of terrestrial and ocean biome reorganizations

Figure 5 shows continuous time-series of the areal extent of terrestrial and oceanic biomes over 1981-2300, estimated from annual mean model output. The most notable contrast between the land and ocean lies in the temporal evolution of their least productive biomes. Consistent with previous studies, terrestrial biomes respond linearly to increasing greenhouse gas forcing (Mahlstein et al., 2013). On the contrary, oligotrophic ocean biomes remain largely unchanged through 2100, despite gradual increases in ocean warming and upper-ocean stratification (Lee et al., 2025). This apparent resilience does not persist beyond 2100, when oligotrophic biomes expand rapidly, reaching 18% of the global ocean surface (Fig. 5b), accompanied by poleward expansion of submesotrophic biomes (Figs. 4c and 4d).

https://doi.org/10.5194/egusphere-2026-1920
Preprint. Discussion started: 18 May 2026

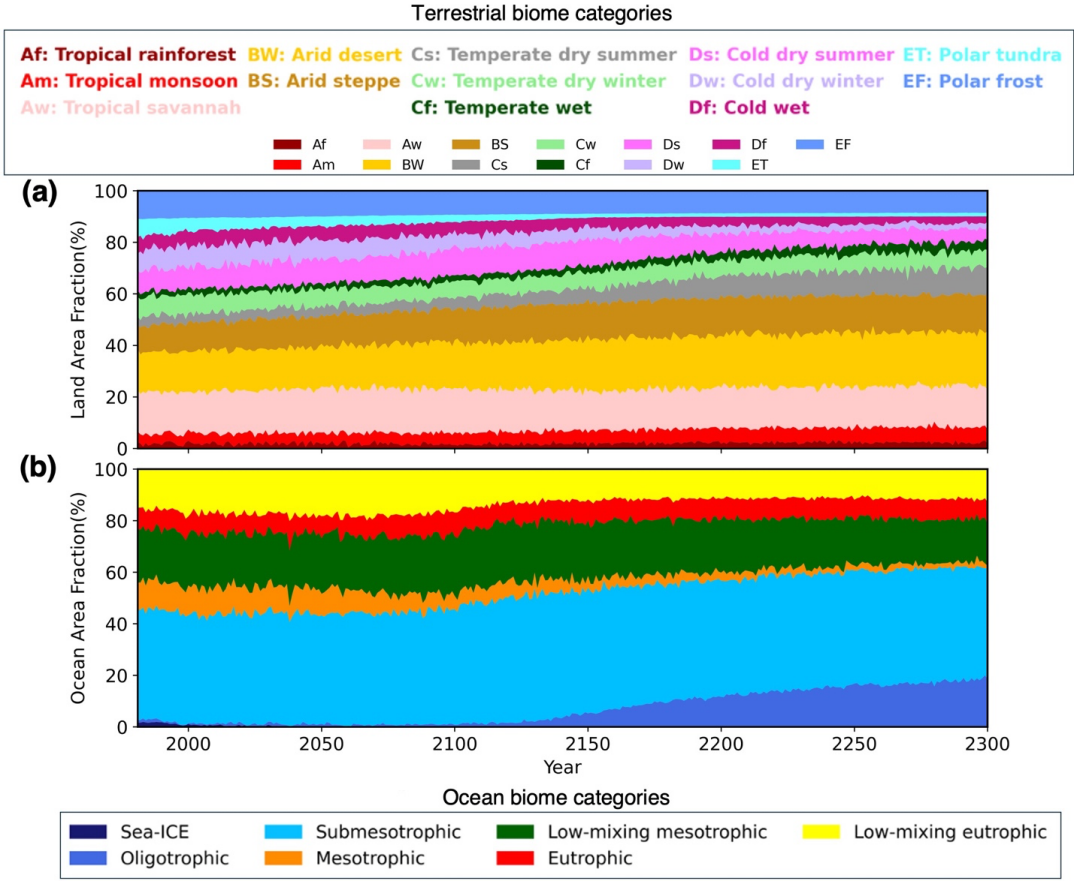

Figure 5: Simulated temporal evolution of global biome fractional areas. Time-series displaying temporal changes in the fractional global land and ocean area occupied by each biome for (a) land and (b) ocean. Biome categories are color-coded as indicated (a) above and (b) below panel.

This delayed and non-linear oceanic response is attributable to the adaptive capacity of phytoplankton under nutrient stress. When ambient inorganic nutrient concentrations are low, phytoplankton can access essential nutrients through processes such as N_2 fixation (Fig. S6) and enhanced recycling of organic matter (Bopp et al., 2022; Sreeush et al., 2024; Letscher and Moore, 2015). In addition, phytoplankton can regulate cellular stoichiometry by reducing phosphorus requirements while sustaining carbon fixation, a process referred to as carbon-to-phosphorus (C:P) plasticity (Kwon et al., 2022; Tanioka and Matsumoto, 2017; Martiny et al., 2022; Galbraith and Martiny, 2015). Consistent with this mechanism, simulations without C:P plasticity (Kwon et al., 2022) show oligotrophic regions expanding from ~1% at present to ~8% by 2100 (Fig. S10), whereas inclusion of C:P plasticity yields an almost invariant response over the same period. These adaptive strategies delay the onset of nutrient depletion, but only while surface phosphate concentrations remain above a near-zero critical threshold. Once sustained biological uptake and persistent stratification drive widespread phosphate limitation (Fig. S11), this buffering capacity breaks down. This

https://doi.org/10.5194/egusphere-2026-1920
Preprint. Discussion started: 18 May 2026

behavior differs from systems limited by iron or nitrogen, where external inputs—such as atmospheric Fe deposition or biological N_2 fixation—can partially offset nutrient deficits. In contrast, external phosphate supply is much more limited (Paytan and Mclaughlin, 2007), leading to a rapid and large-scale transition toward oligotrophic conditions across much of the global ocean.

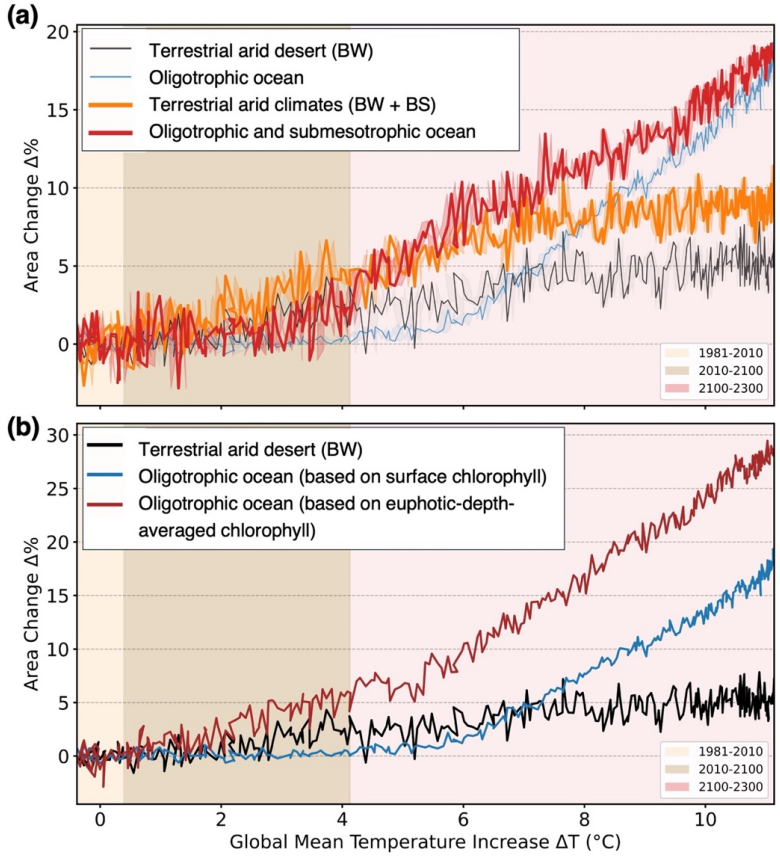

Figure 6: Sensitivity of the least productive terrestrial and ocean biome areas to global surface warming. Plots show the projected changes relative to the present-day conditions in fractional area (%) of global land or ocean as a function of global mean surface temperature increase (°C). (a) Black and blue lines show the areal extent of the terrestrial arid desert (BW) and oligotrophic ocean biomes, respectively. Orange and red lines show the extent of arid climates (BW + BS) and the combined oligotrophic and submesotrophic ocean biomes. Solid lines represent the mean of the 10-member ensemble, and shading denotes ± standard deviation across ensemble members. Three distinct time periods are indicated by different background shading, as shown in the legend at the bottom right of each panel. (b) Black and blue lines are identical to those shown in (a). Oligotrophic ocean biomes in the blue line are classified using surface chlorophyll. For comparison, the red line shows the extent of oligotrophic ocean biomes classified using euphotic-depth-averaged chlorophyll. Only ensemble means are shown in this panel.

https://doi.org/10.5194/egusphere-2026-1920
Preprint. Discussion started: 18 May 2026

The contrasting responses of terrestrial and ocean biomes to greenhouse warming are further elucidated by examining the relationship between globally integrated biome areas and global mean surface temperature. Terrestrial arid desert area increases approximately linearly with warming up to approximately 8°C above present-day levels, after which the expansion rate diminishes (Fig. 6a). This apparent saturation may reflect the comparatively delayed warming of ocean relative to land (Armour et al., 2016), which indirectly controls further terrestrial biome redistribution. In contrast, the areal extent of oligotrophic ocean biome remains nearly constant until global warming exceeds ~6°C, beyond which it increases sharply, reaching nearly 20% of the global ocean surface at 11°C of warming. A Harvey–Collier linearity test confirms that terrestrial desert expansion is statistically linear ($p = 0.053$), whereas oligotrophic ocean expansion exhibits strong nonlinearity ($p < 0.05$). This qualitative contrast persists even when broader biome categories are considered (combined arid deserts and arid steppes on land; combined oligotrophic and submesotrophic biomes in the ocean), although the threshold for the rapid oceanic response shifts to approximately 3°C.

The robustness of this nonlinear oceanic response is further supported by applying an alternative biome classification based on euphotic-depth-averaged chlorophyll (Fig. 6b). Under this metric, oligotrophic expansion also occurs in two steps with an initial increase of roughly 4% points for up to ~5°C of warming, followed by a more pronounced expansion of roughly 16% point over the subsequent ~5 °C warming. Compared with surface chlorophyll, euphotic-depth–averaged chlorophyll exhibits reduced earlier resilience, potentially reflecting a stronger dependence of lower-euphotic-zone productivity on circulation-driven nutrient supply. Despite these differences in magnitude and timing, the emergent nonlinearity is fundamentally governed by phytoplankton adaptive processes, highlighting a distinct feature of ocean biome responses to sustained climate change.

6 Discussions and conclusions

The joint analysis of terrestrial and oceanic biomes over the extended period 1981-2300 under the SSP3-7.0 scenario reveals emergent features that only become apparent beyond the 21st century. In both domains, the most rapid responses occur in high-latitude and high-altitude cryosphere biomes: terrestrial polar tundra and sea-ice biomes. The sea-ice biome is projected to disappear before 2050 as polar oceans become seasonally ice-free, whereas terrestrial polar tundra continues to retreat until around 2150, coinciding with the projected loss of near-surface permafrost. In contrast, polar frost biomes in Greenland and Antarctica exhibit limited response on multi-centennial timescales, although this muted response partly reflects the absence of dynamic icesheet-climate coupling in our simulations. Because ice-associated biomes support uniquely adapted ecosystems, including ice algae, krill, and penguins, their loss represents a substantial threat to global biodiversity.

Beyond polar regions, our results indicate that Earth's surface becomes progressively less habitable under sustained greenhouse forcing. The globally integrated response of terrestrial desert area to warming is approximately linear in both time and global mean surface temperature. As aridity thresholds rise and precipitation declines, deserts expand steadily, ultimately occupying ~20% of global land area in the extended future. In contrast, the expansion of oligotrophic ocean biomes is initially buffered despite rising temperatures and enhanced upper-ocean stratification. This resilience persists until approximately 2100, owing to phytoplankton's adaptive strategies, including N_2 fixation,

https://doi.org/10.5194/egusphere-2026-1920
Preprint. Discussion started: 18 May 2026

enhanced recycling of organic nutrients, and stoichiometric plasticity. However, once global warming exceeds roughly 5–6°C, widespread phosphorus limitation constrains phytoplankton productivity, leading to a rapid expansion of extreme oligotrophic regions that ultimately cover approximately 18–44% of the global ocean surface. The range reflects uncertainty associated with biome classification based on surface versus euphotic-depth–averaged chlorophyll.

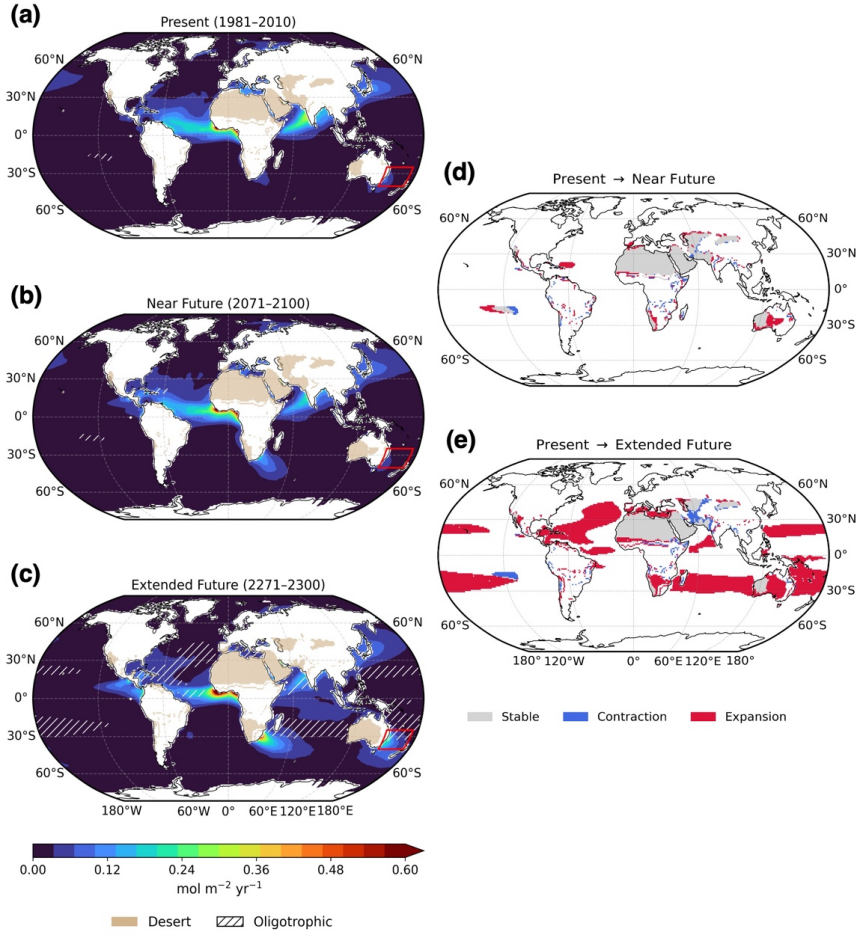

Figure 7: Composite distribution of terrestrial desert and oligotrophic ocean biomes in relation to simulated soluble iron deposition. (a–c) Spatial composites of terrestrial arid deserts (beige shading) and oligotrophic ocean biomes (white hatching) for the (a) present-day, (b) near-future, and (c) extended-future periods, overlaid with simulated soluble iron flux from atmosphere to the ocean surface (mol·m^{-2}yr^{-1}). The red rectangle in the Tasmanian Sea, off eastern Australia, denotes the region over which iron deposition and surface chlorophyll are averaged in Figure 8. (d-e) Changes in arid deserts and oligotrophic ocean biomes relative to present-day conditions for the (d) near-future and (e) extended-future periods. Red shading indicates biome expansion between periods, while blue shading indicates biome contraction. Grey shading denotes regions that persist across both periods.

https://doi.org/10.5194/egusphere-2026-1920
Preprint. Discussion started: 18 May 2026

We refer to this long-term degradation as “compound desertification”, a process characterized by gradual expansion of terrestrial desert followed by an abrupt acceleration of ocean oligotrophication. By the extended future, both terrestrial arid deserts and oligotrophic ocean biomes become concentrated in subtropical belts near 30°N and 30°S, forming a coupled terrestrial-marine desert zone (Fig. 7). This expansion spans much of the subtropical gyres, extending from western boundary currents to eastern ocean basins. Particularly pronounced transitions occur in the mid-latitude North Atlantic (30-45ºN), where regions presently characterized by eutrophic conditions shift toward oligotrophy (Fig. 4d). Together, terrestrial and ocean desertification across the subtropics—covering nearly 40% of Earth’s surface between 30°N and 30°S (Fig. 7c)—poses substantial risks to food security, as both land and ocean become less suitable for supporting crops and wild fisheries. Hotspots of compound desertification include the Mediterranean, Central America, southern Africa, and western Australia—regions already highly vulnerable to climate change.

Integrating terrestrial and ocean biomes further enables assessment of cross-domain feedbacks between land and ocean systems. A key example is aeolian iron deposition, which responds to terrestrial desertification and, in turn, regulates primary productivity in HNLC regions (Weis et al., 2024). Our simulations suggest that increased aridity (e.g., terrestrial desert expansion) enhances downwind iron deposition, most notably over the eastern equatorial Pacific and the oceans off southeastern Australia and southern Africa (Figs. 7a–c). In these regions, increased iron supply can promote phytoplankton growth and delay or prevent transitions toward oligotrophic states. While a fully quantitative assessment of this feedback would require dedicated sensitivity experiments (e.g., suppressing aeolian dust inputs), our 10-member ensemble enables us to infer the strength of coupling associated with internal variability. To this end, we examine 30-year averages of changes in iron deposition versus changes in surface chlorophyll for the near and extended future relative to present-day conditions across ensemble members (Fig. 8). By isolating the ensemble spread arising from internal variability, correlations across ensemble members provide a measure of the strength of this coupling.

A positive correlation ($r = 0.68$; $p < 0.01$) is found in the downwind region of Australian deserts during the near-future period, indicating that regional desert expansion can directly enhance surface chlorophyll associated with small phytoplankton (Fig. 8a). However, this relationship weakens in the extended future (Fig. 8b), as increasing phosphate limitation reduces the effectiveness of additional iron inputs in stimulating productivity. Beyond classical HNLC regions, enhanced iron availability supports N_2-fixing diazotrophs (Wu et al., 2000), sustaining elevated nitrogen fixation (Fig. S6). At the global scale, this is reflected in weak but generally positive correlations—significant at $p < 0.1$ for some phytoplankton groups—between changes in iron deposition and chlorophyll. However, this coupling is partially obscured by competition among phytoplankton groups for shared resources, as well as by other limiting factors such as light and macronutrient availability. For example, no significant correlation ($p < 0.1$) is found between globally averaged small phytoplankton chlorophyll and iron deposition across future simulations, despite the locally significant relationship estimated over the Tasman Sea in the near future.

https://doi.org/10.5194/egusphere-2026-1920
Preprint. Discussion started: 18 May 2026

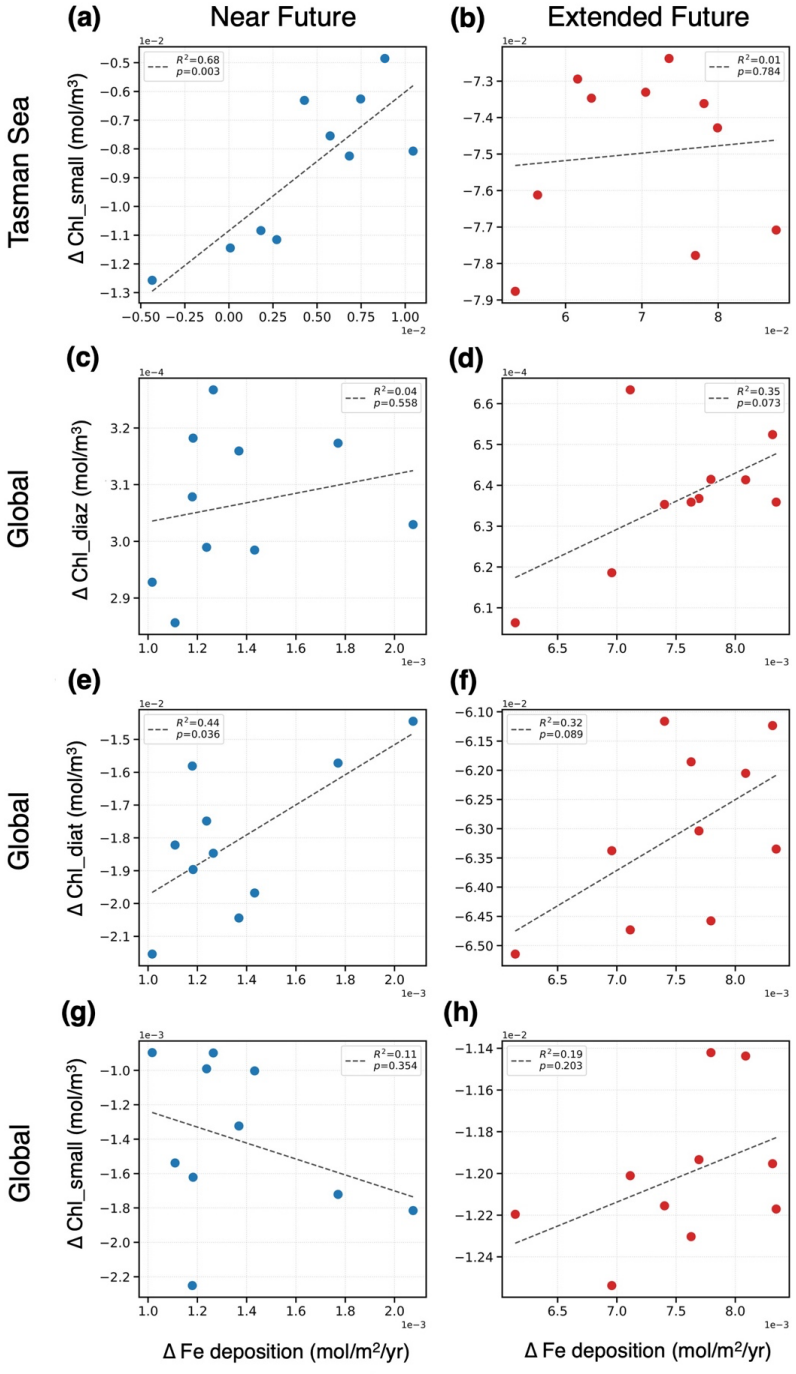

559

560 **Figure 8:** Relationship between changes in surface chlorophyll and aeolian iron (Fe) deposition. Changes are shown
561 for the near and extended future relative to present-day conditions across 10 ensemble members. (a–b) Relationships

https://doi.org/10.5194/egusphere-2026-1920
Preprint. Discussion started: 18 May 2026

562 for small phytoplankton chlorophyll (Chl_small) averaged over the Tasman Sea region off eastern Australia. (c–h)
563 Relationships for (c,d) diazotrophs chlorophyll (Chl_diaz), (e,f) diatoms chlorophyll (Chl_diat), and (g,h) small
564 phytoplankton chlorophyll (Chl_small) averaged over the global ocean. The left column shows the near-future period
565 (2071–2100), and the right column shows the extended-future period (2271–2300). Each dot represents an individual
566 ensemble member. Black dashed lines indicate linear regressions. The coefficient of determination (R^2) and
567 corresponding p-value are reported in each panel.

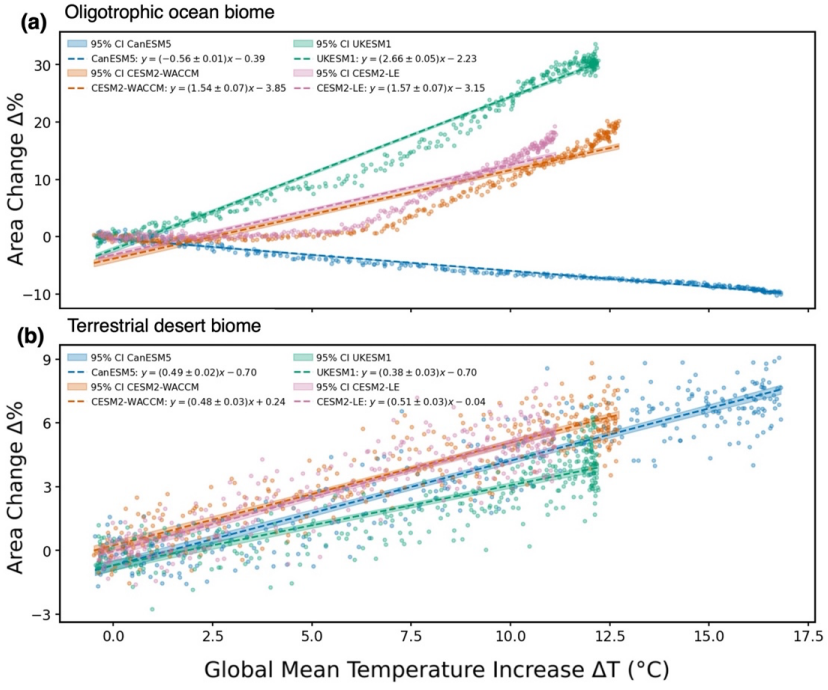

568

569 **Figure 9:** Sensitivity of the least productive terrestrial and ocean biome areas to global surface warming across four
570 Earth system models. Scatter plots show simulated changes in fractional area (%) as a function of global mean
571 temperature increase (°C) for (a) oligotrophic ocean biomes and (b) terrestrial arid deserts. Each scatter corresponds
572 to annual mean estimate. Results are shown for four models: CanESM5 (blue), UKESM1 (green), CESM2-WACCM
573 (orange), and CESM2-CAM (or CESM2-LE, pink), the latter being the primary model used in this study. Dashed lines
574 denote linear regressions fitted to the scatter points, with shading denoting the 95% confidence intervals (CI).
575 Corresponding linear regression equations are reported in the legends.

576 Inter-model comparisons across three Earth system models reveal substantial uncertainty in projected biome
577 responses. Terrestrial biome redistribution primarily reflects differences in climate sensitivity and associated regional
578 temperature and precipitation patterns. Nevertheless, all models consistently simulate expansion of terrestrial arid
579 deserts that scales approximately linearly with global warming (Fig. 9b). On the contrary, both present-day
580 distributions and future trajectories of ocean biomes are highly model dependent (Figs. 9a and S12). For instance,

https://doi.org/10.5194/egusphere-2026-1920
Preprint. Discussion started: 18 May 2026

CanESM5 simulates a linear contraction rather than non-linear expansion of oligotrophic regions, partly due to warming-induced increases in organic matter remineralization rates (Christian et al., 2022). Enhanced remineralization increases nutrient recycling within the twilight zone, and subsequent entrainment into the euphotic zone partially counteracts stratification-driven oligotrophication (Rodgers et al., 2024). By contrast, UKESM1, which lacks C:P plasticity in phytoplankton stoichiometry (Yool et al., 2013), exhibits a more linear expansion of oligotrophic waters with surface warming, without the pronounced resilience phase simulated by CESM2. CESM2-WACCM, having the same biogeochemical component as CESM2-CAM but including interactive stratospheric chemistry and stronger radiative forcing, replicates similar threshold behavior.

These inter-model contrasts underscore the dominant role of poorly constrained biogeochemical processes—particularly nutrient cycling, remineralization dynamics, and phytoplankton stoichiometric flexibility—in shaping long-term marine ecosystem responses. Improved observational constraints and more realistic representation of marine biogeochemistry remain critical priorities for Earth system modeling.

Despite these uncertainties, the projected reorganization of global biomes implies substantial long-term risks to food security and socio-economic stability. Regions already vulnerable to water scarcity and food insecurity—including the Mediterranean, southern Africa, and Central America—are likely to experience compound desertification across both land and adjacent ocean systems. In the marine realm, rapid expansion of oligotrophic biomes may emerge as a central driver of ecosystem redistribution beyond 2100, interacting with concurrent stressors such as warming, acidification, and deoxygenation. Notably, the nonlinear nature of oligotrophic expansion suggests that the ocean carbon sink may appear resilient for decades before weakening abruptly, introducing a delayed but potentially powerful positive climate feedback. This delayed yet abrupt ecological transition carries profound implications for fisheries, ocean-based livelihoods, and intergenerational climate risk. Effective mitigation and adaptation strategies must therefore account for multi-centennial oceanic tipping dynamics that may unfold beyond the 21st century yet commit future generations to enduring environmental change.

Code and data availability

The CESM2 code is available at https://www.cesm.ucar.edu/models/cesm2 (last access: 26 August 2025). The CESM2 simulations are made available at https://climatedata.ibs.re.kr/data/papers/lee-et-al-2025-earth-system-dynamics. ERA-5 datasets are from https://cds.climate.copernicus.eu. The SeaWiFS chlorophyll data are from http://oceandata.sci.gsfc.nasa.gov/. The sea ice concentration data are available at https://data.marine.copernicus.eu/product/GLOBAL_MULTIYEAR_PHY_ENS_001_031/description.

Supplement link

Author contributions

EYK designed the study. DP analyzed both observational and model data to assess ocean biome changes and produced most of the figures, while EJP conducted the land biome analyses and generated the corresponding figures.

https://doi.org/10.5194/egusphere-2026-1920
Preprint. Discussion started: 18 May 2026

EYK led the manuscript preparation with inputs from DP, EJP, and SJ. All authors contributed to the interpretation of the results and to editing the final manuscript.

Competing interests

The authors declare there are no conflicts of interest for this manuscript.

Acknowledgments

We thank Sun-Seon Lee and Axel Timmerman for discussions throughout the work.

Financial support

This work was supported by a 2-Year Research Grant of Pusan National University.

References

Armour, K. C., Marshall, J., Scott, J. R., Donohoe, A., and Newsom, E. R.: Southern Ocean warming delayed by circumpolar upwelling and equatorward transport, Nature Geoscience, 9, 549-554, https://doi.org/10.1038/ngeo2731, 2016.

Beaugrand, G., Reid, P. C., Ibañez, F., Lindley, J. A., and Edwards, M.: Reorganization of North Atlantic Marine Copepod Biodiversity and Climate, Science, 296, 1692-1694, https://doi.org/doi:10.1126/science.1071329, 2002.

Beck, H. E., McVicar, T. R., Vergopolan, N., Berg, A., Lutsko, N. J., Dufour, A., Zeng, Z., Jiang, X., van Dijk, A. I. J. M., and Miralles, D. G.: High-resolution (1 km) Köppen-Geiger maps for 1901–2099 based on constrained CMIP6 projections, Scientific Data, 10, 724, https://doi.org/10.1038/s41597-023-02549-6, 2023.

Benedetti, F., Vogt, M., Elizondo, U. H., Righetti, D., Zimmermann, N. E., and Gruber, N.: Major restructuring of marine plankton assemblages under global warming, Nature Communications, 12, 5226, https://doi.org/10.1038/s41467-021-25385-x, 2021.

Berg, A., de Noblet-Ducoudré, N., Sultan, B., Lengaigne, M., and Guimberteau, M.: Projections of climate change impacts on potential C4 crop productivity over tropical regions, Agricultural and Forest Meteorology, 170, 89-102, https://doi.org/https://doi.org/10.1016/j.agrformet.2011.12.003, 2013.

Bopp, L., Aumont, O., Kwiatkowski, L., Clerc, C., Dupont, L., Ethé, C., Séférian, R., and Tagliabue, A.: Diazotrophy as a key driver of the response of marine net primary productivity to climate change, Biogeosciences, 19, 4267-4285, https://doi.org/10.5194/bg-19-4267-2022, 2022.

Bopp, L., Resplandy, L., Orr, J. C., Doney, S. C., Dunne, J. P., Gehlen, M., Halloran, P., Heinze, C., Ilyina, T., Seferian, R., Tjiputra, J., and Vichi, M.: Multiple stressors of ocean ecosystems in the 21st century: projections with CMIP5 models, Biogeosciences, 10, 6225-6245, https://doi.org/10.5194/bg-10-6225-2013, 2013.

Boyce, D. G., Lewis, M. R., and Worm, B.: Global phytoplankton decline over the past century, Nature, 466, 591-596, https://doi.org/10.1038/nature09268, 2010.

Burrows, M. T., Schoeman, D. S., Buckley, L. B., Moore, P., Poloczanska, E. S., Brander, K. M., Brown, C., Bruno, J. F., Duarte, C. M., Halpern, B. S., Holding, J., Kappel, C. V., Kiessling, W., O'Connor, M. I., Pandolfi, J. M., Parmesan, C., Schwing, F. B., Sydeman, W. J., and Richardson, A. J.: The Pace of Shifting Climate in Marine and Terrestrial Ecosystems, Science, 334, 652-655, https://doi.org/doi:10.1126/science.1210288, 2011.

https://doi.org/10.5194/egusphere-2026-1920
Preprint. Discussion started: 18 May 2026

650 Cho, H.-M., Kim, G., Kwon, E. Y., Moosdorf, N., Garcia-Orellana, J., and Santos, I. R.: Radium tracing nutrient
651 inputs through submarine groundwater discharge in the global ocean, Scientific Reports, 8, 2439,
652 https://doi.org/10.1038/s41598-018-20806-2, 2018.

653 Christian, J. R., Denman, K. L., Hayashida, H., Holdsworth, A. M., Lee, W. G., Riche, O. G. J., Shao, A. E., Steiner,
654 N., and Swart, N. C.: Ocean biogeochemistry in the Canadian Earth System Model version 5.0.3: CanESM5 and
655 CanESM5-CanOE, Geosci. Model Dev. , 15, 4393-4424, https://doi.org/10.5194/gmd-15-4393-2022, 2022.

656 Cornec, M., Claustre, H., Mignot, A., Guidi, L., Lacour, L., Poteau, A., D'Ortenzio, F., Gentili, B., and Schmechtig,
657 C.: Deep Chlorophyll Maxima in the Global Ocean: Occurrences, Drivers and Characteristics, Global
658 Biogeochemical Cycles, 35, e2020GB006759, https://doi.org/https://doi.org/10.1029/2020GB006759, 2021.

659 Cullen, J. J.: Subsurface Chlorophyll Maximum Layers: Enduring Enigma or Mystery Solved?, Annual Review of
660 Marine Science, 7, 207-239, https://doi.org/https://doi.org/10.1146/annurev-marine-010213-135111, 2015.

661 Danabasoglu, G., Lamarque, J. F., Bacmeister, J., Bailey, D. A., DuVivier, A. K., Edwards, J., Emmons, L. K.,
662 Fasullo, J., Garcia, R., Gettelman, A., Hannay, C., Holland, M. M., Large, W. G., Lauritzen, P. H., Lawrence, D. M.,
663 Lenaerts, J. T. M., Lindsay, K., Lipscomb, W. H., Mills, M. J., Neale, R., Oleson, K. W., Otto-Bliesner, B., Phillips,
664 A. S., Sacks, W., Tilmes, S., van Kampenhout, L., Vertenstein, M., Bertini, A., Dennis, J., Deser, C., Fischer, C.,
665 Fox-Kemper, B., Kay, J. E., Kinnison, D., Kushner, P. J., Larson, V. E., Long, M. C., Mickelson, S., Moore, J. K.,
666 Nienhouse, E., Polvani, L., Rasch, P. J., and Strand, W. G.: The Community Earth System Model Version 2
667 (CESM2), J. Adv. Mod. Earth Syst., 12, e2019MS001916, https://doi.org/10.1029/2019MS001916, 2020.

668 de Boyer montégut, C.: Mixed layer depth climatology computed with a density threshold criterion of 0.03kg/m3
669 from 10 m depth value [dataset], 10.17882/91774, 2023.

670 de Boyer Montégut, C., Madec, G., Fischer, A. S., Lazar, A., and Iudicone, D.: Mixed layer depth over the global
671 ocean: An examination of profile data and a profile-based climatology, Journal of Geophysical Research: Oceans,
672 109, https://doi.org/https://doi.org/10.1029/2004JC002378, 2004.

673 Eyring, V., Bony, S., Meehl, G. A., Senior, C. A., Stevens, B., Stouffer, R. J., and Taylor, K. E.: Overview of the
674 Coupled Model Intercomparison Project Phase 6 (CMIP6) experimental design and organization, Geosci. Model
675 Dev., 9, 1937-1958, https://doi.org/10.5194/gmd-9-1937-2016, 2016.

676 Fay, A. R. and McKinley, G. A.: Global open-ocean biomes: mean and temporal variability, Earth Syst. Sci. Data, 6,
677 273-284, 2014.

678 Feng, S. and Fu, Q.: Expansion of global drylands under a warming climate, Atmos. Chem. Phys., 13, 10081-10094,
679 https://doi.org/10.5194/acp-13-10081-2013, 2013.

680 Fung, I. Y., Doney, S. C., Lindsay, K., and John, J.: Evolution of carbon sinks in a changing climate, Proceedings of
681 the National Academy of Sciences, 102, 11201-11206, https://doi.org/doi:10.1073/pnas.0504949102, 2005.

682 Galbraith, E. D. and Martiny, A. C.: A simple nutrient-dependence mechanism for predicting the stoichiometry of
683 marine ecosystems, Proc. Natl. Acad. Sci. U.S.A., 112, 8199-8204, https://doi.org/10.1073/pnas.1423917112, 2015.

684 Geiger, R.: Klassifikation der Klimate nach W. Köppen, in: Landolt-Börnstein – Zahlenwerte und Funktionen aus
685 Physik, Chemie, Astronomie, Geophysik und Technik, Springer, 603-607, 1954.

686 Harsch, M. A., Hulme, P. E., McGlone, M. S., and Duncan, R. P.: Are treelines advancing? A global meta-analysis
687 of treeline response to climate warming, Ecology Letters, 12, 1040-1049,
688 https://doi.org/https://doi.org/10.1111/j.1461-0248.2009.01355.x, 2009.

689 Held, I. M. and Soden, B. J.: Robust Responses of the Hydrological Cycle to Global Warming, Journal of Climate,
690 19, 5686-5699, https://doi.org/https://doi.org/10.1175/JCLI3990.1, 2006.

https://doi.org/10.5194/egusphere-2026-1920
Preprint. Discussion started: 18 May 2026

691 Henson, S. A., Cael, B. B., Allen, S. R., and Dutkiewicz, S.: Future phytoplankton diversity in a changing climate,
692 Nature Communications, 12, 5372, https://doi.org/10.1038/s41467-021-25699-w, 2021.

693 Hersbach, H., Bell, B., Berrisford, P., Hirahara, S., Horányi, A., Muñoz-Sabater, J., Nicolas, J., Peubey, C., Radu,
694 R., Schepers, D., Simmons, A., Soci, C., Abdalla, S., Abellan, X., Balsamo, G., Bechtold, P., Biavati, G., Bidlot, J.,
695 Bonavita, M., De Chiara, G., Dahlgren, P., Dee, D., Diamantakis, M., Dragani, R., Flemming, J., Forbes, R.,
696 Fuentes, M., Geer, A., Haimberger, L., Healy, S., Hogan, R. J., Hólm, E., Janisková, M., Keeley, S., Laloyaux, P.,
697 Lopez, P., Lupu, C., Radnoti, G., de Rosnay, P., Rozum, I., Vamborg, F., Villaume, S., and Thépaut, J.-N.: The
698 ERA5 global reanalysis, Quarterly Journal of the Royal Meteorological Society, 146, 1999-2049,
699 https://doi.org/https://doi.org/10.1002/qj.3803, 2020.

700 Huang, J., Yu, H., Guan, X., Wang, G., and Guo, R.: Accelerated dryland expansion under climate change, Nature
701 Climate Change, 6, 166-171, https://doi.org/10.1038/nclimate2837, 2016.

702 Hunke, E. C., Lipscomb, W. H., Turner, A. K., Jeffery, N., and Elliott, S.: CICE: The Los Alamos Sea Ice Model.
703 Documentation and Software User's Manual. Version 5.1., Los Alamos National Laboratory, 2015.

704 Irwin, A. J. and Oliver, M. J.: Are ocean deserts getting larger?, Geophysical Research Letters, 36,
705 https://doi.org/https://doi.org/10.1029/2009GL039883, 2009.

706 Kaplan, J. O., Bigelow, N. H., Prentice, I. C., Harrison, S. P., Bartlein, P. J., Christensen, T. R., Cramer, W.,
707 Matveyeva, N. V., McGuire, A. D., Murray, D. F., Razzhivin, V. Y., Smith, B., Walker, D. A., Anderson, P. M.,
708 Andreev, A. A., Brubaker, L. B., Edwards, M. E., and Lozhkin, A. V.: Climate change and Arctic ecosystems: 2.
709 Modeling, paleodata-model comparisons, and future projections, Journal of Geophysical Research: Atmospheres,
710 108, https://doi.org/https://doi.org/10.1029/2002JD002559, 2003.

711 Kelly, A. E. and Goulden, M. L.: Rapid shifts in plant distribution with recent climate change, Proceedings of the
712 National Academy of Sciences, 105, 11823-11826, https://doi.org/doi:10.1073/pnas.0802891105, 2008.

713 Kim, I.-W., Timmermann, A., Kim, J.-E., Rodgers, K. B., Lee, S.-S., Lee, H., and Wieder, W. R.: Abrupt increase in
714 Arctic-Subarctic wildfires caused by future permafrost thaw, Nature Communications, 15, 7868,
715 https://doi.org/10.1038/s41467-024-51471-x, 2024.

716 Köppen, W. D.: Wärmezonen der Erde, nach der Dauer der heissen, gemässigten und kalten Zeit und nach der
717 Wirkung der Wärme auf die organische Welt betrachtet., Meteorologische Zeitschrift, 1, 215-226, 1884.

718 Koven, C. D., Arora, V. K., Cadule, P., Fisher, R. A., Jones, C. D., Lawrence, D. M., Lewis, J., Lindsay, K.,
719 Mathesius, S., Meinshausen, M., Mills, M., Nicholls, Z., Sanderson, B. M., Séférian, R., Swart, N. C., Wieder, W.
720 R., and Zickfeld, K.: Multi-century dynamics of the climate and carbon cycle under both high and net negative
721 emissions scenarios, Earth Syst Dynam, 13, 885-909, https://doi.org/10.5194/esd-13-885-2022, 2022.

722 Kug, J.-S., Oh, J.-H., An, S.-I., Yeh, S.-W., Min, S.-K., Son, S.-W., Kam, J., Ham, Y.-G., and Shin, J.: Hysteresis of
723 the intertropical convergence zone to CO2 forcing, Nature Climate Change, 12, 47-53,
724 https://doi.org/10.1038/s41558-021-01211-6, 2022.

725 Kwiatkowski, L., Torres, O., Bopp, L., Aumont, O., Chamberlain, M., Christian, J. R., Dunne, J. P., Gehlen, M.,
726 Ilyina, T., John, J. G., Lenton, A., Li, H. M., Lovenduski, N. S., Orr, J. C., Palmieri, J., Santana-Falcon, Y.,
727 Schwinger, J., Seferian, R., Stock, C. A., Tagliabue, A., Takano, Y., Tjiputra, J., Toyama, K., Tsujino, H.,
728 Watanabe, M., Yamamoto, A., Yool, A., and Ziehn, T.: Twenty-first century ocean warming, acidification,
729 deoxygenation, and upper-ocean nutrient and primary production decline from CMIP6 model projections,
730 Biogeosciences, 17, 3439-3470, https://doi.org/10.5194/bg-17-3439-2020, 2020.

731 Kwon, E. Y., Sreeush, M. G., Timmermann, A., Karl, D. M., Church, M. J., Lee, S.-S., and Yamaguchi, R.: Nutrient
732 uptake plasticity in phytoplankton sustains future ocean net primary production, Sci. Adv., 8, eadd2475,
733 https://doi.org/10.1126/sciadv.add2475, 2022.

https://doi.org/10.5194/egusphere-2026-1920
Preprint. Discussion started: 18 May 2026

734 Laufkötter, C., Vogt, M., Gruber, N., Aita-Noguchi, M., Aumont, O., Bopp, L., Buitenhuis, E., Doney, S. C., Dunne,
735 J., Hashioka, T., Hauck, J., Hirata, T., John, J., Le Quéré, C., LIma, I. D., Nakano, H., Sefeian, R., Totterdell, I.,
736 Vichi, M., and Völker, C.: Drivers and uncertainties of future global marine primary production in marine ecosystem
737 models, Biogeosciences, 12, 6955-6984, https://doi.org/10.5194/bg-12-6955-2015, 2015.

738 Lawrence, D. M., Hurtt, G. C., Arneth, A., Brovkin, V., Calvin, K. V., Jones, A. D., Jones, C. D., Lawrence, P. J., de
739 Noblet-Ducoudré, N., Pongratz, J., Seneviratne, S. I., and Shevliakova, E.: The Land Use Model Intercomparison
740 Project (LUMIP) contribution to CMIP6: rationale and experimental design, Geosci. Model Dev., 9, 2973-2998,
741 https://doi.org/10.5194/gmd-9-2973-2016, 2016.

742 Lawrence, D. M., Fisher, R. A., Koven, C. D., Oleson, K. W., Swenson, S. C., Bonan, G., Collier, N., Ghimire, B.,
743 van Kampenhout, L., Kennedy, D., Kluzek, E., Lawrence, P. J., Li, F., Li, H., Lombardozzi, D., Riley, W. J., Sacks,
744 W. J., Shi, M., Vertenstein, M., Wieder, W. R., Xu, C., Ali, A. A., Badger, A. M., Bisht, G., van den Broeke, M.,
745 Brunke, M. A., Burns, S. P., Buzan, J., Clark, M., Craig, A., Dahlin, K., Drewniak, B., Fisher, J. B., Flanner, M.,
746 Fox, A. M., Gentine, P., Hoffman, F., Keppel-Aleks, G., Knox, R., Kumar, S., Lenaerts, J., Leung, L. R., Lipscomb,
747 W. H., Lu, Y., Pandey, A., Pelletier, J. D., Perket, J., Randerson, J. T., Ricciuto, D. M., Sanderson, B. M., Slater, A.,
748 Subin, Z. M., Tang, J., Thomas, R. Q., Val Martin, M., and Zeng, X.: The Community Land Model Version 5:
749 Description of New Features, Benchmarking, and Impact of Forcing Uncertainty, Journal of Advances in Modeling
750 Earth Systems, 11, 4245-4287, https://doi.org/https://doi.org/10.1029/2018MS001583, 2019.

751 Lee, S. S., Sharma, S., Rosenbloom, N., Rodgers, K. B., Kim, J. E., Kwon, E. Y., Franzke, C. L. E., Kim, I. W.,
752 Sreeush, M. G., and Stein, K.: Multi-centennial climate change in a warming world beyond 2100, Earth Syst
753 Dynam, 16, 1427-1451, https://doi.org/10.5194/esd-16-1427-2025, 2025.

754 Lenoir, J., Gégout, J. C., Marquet, P. A., de Ruffray, P., and Brisse, H.: A Significant Upward Shift in Plant Species
755 Optimum Elevation During the 20th Century, Science, 320, 1768-1771,
756 https://doi.org/doi:10.1126/science.1156831, 2008.

757 Leonelli, F. E., Bellacicco, M., Pitarch, J., Organelli, E., Buongiorno Nardelli, B., de Toma, V., Cammarota, C.,
758 Marullo, S., and Santoleri, R.: Ultra-Oligotrophic Waters Expansion in the North Atlantic Subtropical Gyre
759 Revealed by 21 Years of Satellite Observations, Geophysical Research Letters, 49, e2021GL096965,
760 https://doi.org/https://doi.org/10.1029/2021GL096965, 2022.

761 Letscher, R. T. and Moore, J. K.: Preferential remineralization of dissolved organic phosphorus and non-Redfield
762 DOM dynamics in the global ocean: Impacts on marine productivity, nitrogen fixation, and carbon export, Global
763 Bigeochem. Cycles, 29, 325-340, https://doi.org/10.1002/2014gb004904, 2015.

764 Lipscomb, W. H., Fyke, J. G., Vizcaíno, M., Sacks, W. J., Wolfe, J., Vertenstein, M., Craig, A., Kluzek, E., and
765 Lawrence, D. M.: Implementation and Initial Evaluation of the Glimmer Community Ice Sheet Model in the
766 Community Earth System Model, Journal of Climate, 26, 7352-7371, https://doi.org/https://doi.org/10.1175/JCLI-D-
767 12-00557.1, 2013.

768 Lipscomb, W. H., Price, S. F., Hoffman, M. J., Leguy, G. R., Bennett, A. R., Bradley, S. L., Evans, K. J., Fyke, J.
769 G., Kennedy, J. H., Perego, M., Ranken, D. M., Sacks, W. J., Salinger, A. G., Vargo, L. J., and Worley, P. H.:
770 Description and evaluation of the Community Ice Sheet Model (CISM) v2.1, Geosci. Model Dev., 12, 387-424,
771 https://doi.org/10.5194/gmd-12-387-2019, 2019.

772 Loarie, S. R., Duffy, P. B., Hamilton, H., Asner, G. P., Field, C. B., and Ackerly, D. D.: The velocity of climate
773 change, Nature, 462, 1052-1055, https://doi.org/10.1038/nature08649, 2009.

774 Lohmann, U., Sausen, R., Bengtsson, L., Cubasch, U., Perlwitz, J., and Roeckner, E.: The Köppen climate
775 classification as a diagnostic tool for general circulation models, Climate Research, 3, 177-193, 1993.

https://doi.org/10.5194/egusphere-2026-1920
Preprint. Discussion started: 18 May 2026

776 Long, M. C., Moore, J. K., Lindsay, K., Levy, M., Doney, S. C., Luo, J. Y., Krumhardt, K. M., Letscher, R. T.,
777 Grover, M., and Sylvester, Z. T.: Simulations with the marine biogeochemistry library (MARBL), J. Adv. Model.
778 Earth Syst. , 13, e2021MS002647, https://doi.org/10.1029/2021MS002647, 2021.

779 Longhurst, A. R.: Ecological geography of the sea (2nd ed.), Academic Press2007.

780 Mahlstein, I., Daniel, J. S., and Solomon, S.: Pace of shifts in climate regions increases with global temperature,
781 Nature Climate Change, 3, 739-743, https://doi.org/10.1038/nclimate1876, 2013.

782 Martiny, A. C., Hagstrom, G. I., DeVries, T., Letscher, R. T., Britten, G. L., Garcia, C. A., Galbraith, E. D., Karl, D.
783 M., Levin, S. A., Lomas, M. W., Moreno, A. R., Talmy, D., Wang, W.-L., and Matsumoto, K.: Marine
784 phytoplankton resilience may moderate oligotrophic ecosystem responses and biogeochemical feedbacks to climate
785 change, Limnol. Oceanogr., 9999, 1-12, https://doi.org/10.1002/lno.12029, 2022.

786 Mayorga, E., Seitzinger, S. P., Harrison, J. A., Dumont, E., Beusen, A. H. W., Bouwman, A. F., Fekete, B. M.,
787 Kroeze, C., and Van Drecht, G.: Global Nutrient Export from WaterSheds 2 (NEWS 2): Model development and
788 implementation, Environ. Modell. Softw., 25, 837-853, https://doi.org/10.1016/j.envsoft.2010.01.007, 2010.

789 Meehl, G. A., Senior, C. A., Eyring, V., Flato, G., Lamarque, J.-F., Stouffer, R. J., Taylor, K. E., and Schlund, M.:
790 Context for interpreting equilibrium climate sensitivity and transient climate response from the CMIP6 Earth system
791 models, Science Advances, 6, eaba1981, https://doi.org/doi:10.1126/sciadv.aba1981, 2020.

792 Meier, W. N., Fetterer, F., Windnagel, A. K., and Stewart, J. S.: Near-Real-Time NOAA/NSIDC Climate Data
793 Record of Passive Microwave Sea Ice Concentration (G10016, Version 2) [dataset], 10.7265/tgam-yv28, 2021.

794 Meinshausen, M., Nicholls, Z. R. J., Lewis, J., Gidden, M. J., Vogel, E., Freund, M., Beyerle, U., Gessner, C.,
795 Nauels, A., Bauer, N., Canadell, J. G., Daniel, J. S., John, A., Krummel, P. B., Luderer, G., Meinshausen, N.,
796 Montzka, S. A., Rayner, P. J., Reimann, S., Smith, S. J., van den Berg, M., Velders, G. J. M., Vollmer, M. K., and
797 Wang, R. H. J.: The shared socio-economic pathway (SSP) greenhouse gas concentrations and their extensions to
798 2500, Geosci. Model Dev., 13, 3571-3605, https://doi.org/10.5194/gmd-13-3571-2020, 2020.

799 Misumi, K., Lindsay, K., Moore, J. K., Doney, S. C., Bryan, F. O., Tsumune, D., and Yoshida, Y.: The iron budget
800 in ocean surface waters in the 20th and 21st centuries: projections by the Community Earth System Model version 1,
801 Biogeosciences, 11, 33-55, https://doi.org/10.5194/bg-11-33-2014, 2014.

802 Moore, J. K., Doney, S. C., and Lindsay, K.: Upper ocean ecosystem dynamics and iron cycling in a global three-
803 dimensional model, Global Bigeochem. Cycles, 18, GB4028, https://doi.org/10.1029/2004GB002220, 2004.

804 O'Neill, B. C., Tebaldi, C., van Vuuren, D. P., Eyring, V., Friedlingstein, P., Hurtt, G., Knutti, R., Kriegler, E.,
805 Lamarque, J. F., Lowe, J., Meehl, G. A., Moss, R., Riahi, K., and Sanderson, B. M.: The Scenario Model
806 Intercomparison Project (ScenarioMIP) for CMIP6, Geosci. Model Dev., 9, 3461-3482,
807 https://doi.org/10.5194/gmd-9-3461-2016, 2016.

808 O'Reilly, J. E., Maritorena, S., Mitchell, B. G., Siegel, D. A., Carder, K. L., Garver, S. A., Kahru, M., and McClain,
809 C.: Ocean color chlorophyll algorithms for SeaWiFS, Journal of Geophysical Research: Oceans, 103, 24937-24953,
810 https://doi.org/https://doi.org/10.1029/98JC02160, 1998.

811 Oliver, M. J. and Irwin, A. J.: Objective global ocean biogeographic provinces, Geophysical Research Letters, 35,
812 https://doi.org/https://doi.org/10.1029/2008GL034238, 2008.

813 Palmiéri, J., Yool, A., Popova, K., and Henson, S.: A marine biomes analysis of UKESM1, 2019.

814 Paytan, A. and McLaughlin, K.: The Oceanic Phosphorus Cycle, Chemical Reviews, 107, 563-576,
815 https://doi.org/10.1021/cr0503613, 2007.

https://doi.org/10.5194/egusphere-2026-1920
Preprint. Discussion started: 18 May 2026

816 Peel, M. C., Finlayson, B. L., and McMahon, T. A.: Updated world map of the Köppen-Geiger climate
817 classification, Hydrol. Earth Syst. Sci., 11, 1633-1644, https://doi.org/10.5194/hess-11-1633-2007, 2007.

818 Peng, Q., Xie, S.-P., and Deser, C.: Collapsed upwelling projected to weaken ENSO under sustained warming
819 beyond the twenty-first century, Nature Climate Change, 14, 815-822, https://doi.org/10.1038/s41558-024-02061-8,
820 2024.

821 Penn, J. L. and Deutsch, C.: Avoiding ocean mass extinction from climate warming, Science, 376, 524-526,
822 https://doi.org/doi:10.1126/science.abe9039, 2022.

823 Polovina, J. J., Howell, E. A., and Abecassis, M.: Ocean's least productive waters are expanding, Geophys. Res.
824 Lett., 35, L03618, https://doi.org/10.1029/2007GL031745, 2008.

825 Randerson, J. T., Lindsay, K., Munoz, E., Fu, W., Moore, J. K., Hoffman, F. M., Mahowald, N. M., and Doney, S.
826 C.: Multicentury changes in ocean and land contributions to the climate-carbon feedback, Global Biogeochemical
827 Cycles, 29, 744-759, https://doi.org/https://doi.org/10.1002/2014GB005079, 2015.

828 Reid, J. L., Brinton, E., Fleminger, A., Venrick, E. L., and McGowan, J. A.: Ocean Circulation and Marine Life, in:
829 Advances in Oceanography, edited by: Charnock, H., and Deacon, G., Springer US, Boston, MA, 65-130,
830 10.1007/978-1-4615-8273-1_3, 1978.

831 Rodgers, K. B., Aumont, O., Toyama, K., Resplandy, L., Ishii, M., Nakano, T., Sasano, D., Bianchi, D., and
832 Yamaguchi, R.: Low-latitude mesopelagic nutrient recycling controls productivity and export, Nature, 632, 802-807,
833 https://doi.org/10.1038/s41586-024-07779-1, 2024.

834 Rodgers, K. B., Lee, S. S., Rosenbloom, N., Timmermann, A., Danabasoglu, G., Deser, C., Edwards, J., Kim, J. E.,
835 Simpson, I. R., Stein, K., Stuecker, M. F., Yamaguchi, R., Bodai, T., Chung, E. S., Huang, L., Kim, W. M.,
836 Lamarque, J. F., Lombardozzi, D. L., Wieder, W. R., and Yeager, S. G.: Ubiquity of human-induced changes in
837 climate variability, Earth Syst Dynam, 12, 1393-1411, https://doi.org/10.5194/esd-12-1393-2021, 2021.

838 Scheffers, B. R., De Meester, L., Bridge, T. C. L., Hoffmann, A. A., Pandolfi, J. M., Corlett, R. T., Butchart, S. H.
839 M., Pearce-Kelly, P., Kovacs, K. M., Dudgeon, D., Pacifici, M., Rondinini, C., Foden, W. B., Martin, T. G., Mora,
840 C., Bickford, D., and Watson, J. E. M.: The broad footprint of climate change from genes to biomes to people,
841 Science, 354, aaf7671, https://doi.org/doi:10.1126/science.aaf7671, 2016.

842 Seager, R., Neelin, D., Simpson, I., Liu, H., Henderson, N., Shaw, T., Kushnir, Y., Ting, M., and Cook, B.:
843 Dynamical and Thermodynamical Causes of Large-Scale Changes in the Hydrological Cycle over North America in
844 Response to Global Warming, Journal of Climate, 27, 7921-7948, https://doi.org/https://doi.org/10.1175/JCLI-D-14-
845 00153.1, 2014.

846 Sellar, A. A., Jones, C. G., Mulcahy, J. P., Tang, Y., Yool, A., Wiltshire, A., O'Connor, F. M., Stringer, M., Hill, R.,
847 Palmieri, J., Woodward, S., de Mora, L., Kuhlbrodt, T., Rumbold, S. T., Kelley, D. I., Ellis, R., Johnson, C. E.,
848 Walton, J., Abraham, N. L., Andrews, M. B., Andrews, T., Archibald, A. T., Berthou, S., Burke, E., Blockley, E.,
849 Carslaw, K., Dalvi, M., Edwards, J., Folberth, G. A., Gedney, N., Griffiths, P. T., Harper, A. B., Hendry, M. A.,
850 Hewitt, A. J., Johnson, B., Jones, A., Jones, C. D., Keeble, J., Liddicoat, S., Morgenstern, O., Parker, R. J., Predoi,
851 V., Robertson, E., Siahaan, A., Smith, R. S., Swaminathan, R., Woodhouse, M. T., Zeng, G., and Zerroukat, M.:
852 UKESM1: Description and Evaluation of the U.K. Earth System Model, Journal of Advances in Modeling Earth
853 Systems, 11, 4513-4558, https://doi.org/https://doi.org/10.1029/2019MS001739, 2019.

854 Sharma, S., Ha, K.-J., Rodgers, K. B., Chung, E.-S., Lee, S.-S., and Nellikkattil, A. B.: Substantial shift in phase and
855 amplitude of Indian rainfall beyond 2100, npj Climate and Atmospheric Science, 8, 236,
856 https://doi.org/10.1038/s41612-025-01126-5, 2025.

857 Smith, R., Jones, P., Briegleb, B., Bryan, F., Danabasoglu, G., Dennis, J., and more: The Parallel Ocean Program
858 (POP) reference manual, Ocean component of the Community Climate System Model (CCSM), 2010.

https://doi.org/10.5194/egusphere-2026-1920
Preprint. Discussion started: 18 May 2026

859 Sreeush, M. G., Kwon, E. Y., Lee, S.-S., and Nellikkattil, A. B.: Anthropogenically driven changes in the carbon to
860 phosphorus ratio of marine dissolved organic matter, Global Bigeochem. Cycles, 38, e2023GB008069,
861 https://doi.org/10.1029/2023GB008069, 2024.

862 Swart, N. C., Cole, J. N. S., Kharin, V. V., Lazare, M., Scinocca, J. F., Gillett, N. P., Anstey, J., Arora, V., Christian,
863 J. R., Hanna, S., Jiao, Y., Lee, W. G., Majaess, F., Saenko, O. A., Seiler, C., Seinen, C., Shao, A., Sigmond, M.,
864 Solheim, L., von Salzen, K., Yang, D., and Winter, B.: The Canadian Earth System Model version 5
865 (CanESM5.0.3), Geosci. Model Dev., 12, 4823-4873, https://doi.org/10.5194/gmd-12-4823-2019, 2019.

866 Tanioka, T. and Matsumoto, K.: Buffering of ocean export production by flexible elemental stoichiometry of
867 particulate organic matter, Global Bigeochem. Cycles, 31, 1528-1542, https://doi.org/10.1002/2017GB005670,
868 2017.

869 Thomas, C. D., Cameron, A., Green, R. E., Bakkenes, M., Beaumont, L. J., Collingham, Y. C., Erasmus, B. F. N.,
870 de Siqueira, M. F., Grainger, A., Hannah, L., Hughes, L., Huntley, B., van Jaarsveld, A. S., Midgley, G. F., Miles,
871 L., Ortega-Huerta, M. A., Townsend Peterson, A., Phillips, O. L., and Williams, S. E.: Extinction risk from climate
872 change, Nature, 427, 145-148, https://doi.org/10.1038/nature02121, 2004.

873 Thomas, M. K., Kremer, C. T., Klausmeier, C. A., and Litchman, E.: A Global Pattern of Thermal Adaptation in
874 Marine Phytoplankton, Science, 338, 1085-1088, https://doi.org/doi:10.1126/science.1224836, 2012.

875 Urban, M. C.: Accelerating extinction risk from climate change, Science, 348, 571-573,
876 https://doi.org/doi:10.1126/science.aaa4984, 2015.

877 Vergés, A., Steinberg, P. D., Hay, M. E., Poore, A. G. B., Campbell, A. H., Ballesteros, E., Heck, K. L., Jr, Booth,
878 D. J., Coleman, M. A., Feary, D. A., Figueira, W., Langlois, T., Marzinelli, E. M., Mizerek, T., Mumby, P. J.,
879 Nakamura, Y., Roughan, M., van Sebille, E., Gupta, A. S., Smale, D. A., Tomas, F., Wernberg, T., and Wilson, S.
880 K.: The tropicalization of temperate marine ecosystems: climate-mediated changes in herbivory and community
881 phase shifts, Proceedings of the Royal Society B: Biological Sciences, 281, https://doi.org/10.1098/rspb.2014.0846,
882 2014.

883 Walther, G.-R., Post, E., Convey, P., Menzel, A., Parmesan, C., Beebee, T. J. C., Fromentin, J.-M., Hoegh-
884 Guldberg, O., and Bairlein, F.: Ecological responses to recent climate change, Nature, 416, 389-395,
885 https://doi.org/10.1038/416389a, 2002.

886 Weis, J., Chase, Z., Schallenberg, C., Strutton, P. G., Bowie, A. R., and Fiddes, S. L.: One-third of Southern Ocean
887 productivity is supported by dust deposition, Nature, 629, 603-608, https://doi.org/10.1038/s41586-024-07366-4,
888 2024.

889 Wu, J. F., Sunda, W., Boyle, E. A., and Karl, D. M.: Phosphate depletion in the western North Atlantic Ocean,
890 Science, 239, 759-762, 2000.

891 Yool, A., Popova, E. E., and Anderson, T. R.: MEDUSA-2.0: an intermediate complexity biogeochemical model of
892 the marine carbon cycle for climate change and ocean acidification studies, Geosci. Model Dev., 6, 1767-1811,
893 https://doi.org/10.5194/gmd-6-1767-2013, 2013.
894